Heliyon 10 (2024) e31967

Contents lists available at ScienceDirect

Heliyon

journal homepage: www.cell.com/heliyon

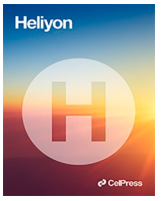

Research article

Adsorption of arsenic and fluoride: Modeling of single and competitive adsorption systems

Amrutha Acharya [a], Gautham Jeppu [a,**], Chikmagalur Raju Girish [a,*], Balakrishna Prabhu [a], Vytla Ramachandra Murty [b,***], Alita Stephy Martis [a], Shrividya Ramesh [a]

[a] Department of Chemical Engineering, Manipal Institute of Technology, Manipal Academy of Higher Education, Manipal, 576104, Karnataka, India
[b] Department of Biotechnology, Manipal Institute of Technology, Manipal Academy of Higher Education, Manipal, 576104, Karnataka, India

ARTICLE INFO

Keywords:
Adsorption
Competitive adsorption
Activated carbon
Arsenic
Fluoride
Competitive adsorption isotherms

ABSTRACT

The elevated co-occurrence of arsenic and fluoride in surface and groundwater poses risks to human health in many parts of the world. Using single and competitive batch equilibrium adsorption studies, this research focuses on As(V) and F adsorption by activated carbon and its modeling. BET, XRD, FESEM, EDS, and FTIR analysis were used to discern the structural characteristics of activated carbon. The influence of dosage, pH, and contact time were also investigated in single and simultaneous adsorption systems. The maximum adsorption capacity of activated carbon for arsenic and fluoride were found to be 3.58 mg/g and 2.32 mg/g, respectively. Kinetics studies indicated that pseudo-second-order kinetic model fit better than pseudo-first-order, Elovich, and intraparticle diffusion kinetic models. The non-linear regression analysis of Langmuir, Freundlich, Toth, Redlich Petersons, and Modified Langmuir Freundlich models was used to determine single-component asorption model parameters. Additionally, the simultaneous adsorption was rigorously modeled and compared using the Extended Langmuir (EL), Extended Langmuir Freundlich (ELF), Modified Competitive Langmuir (MCL), and Jeppu Amrutha Manipal Multicomponent (JAMM) isotherm models, and competitive mechanisms were interpreted for the simultaneous adsorption system. Further, the model performances were evaluated by statistical error analysis using the normalized average percentage error (NAPE), root mean square errors (RMSE), and the correlation coefficient (R^2). According to the modeling results, single equilibrium data fitted better with the Modified Langmuir Freundlich isotherm model, with a higher R^2 of 0.99 and lower NAPE values of 3.8 % and 1.28 % for As(V) and F, than other models. For the binary adsorption, the Extended Langmuir Freundlich isotherm model demonstrated excellent fit with lowest errors. All the competitive isotherm models fit the As(V) and F simultaneous sorption systems reasonably well. Furthermore, the research unveiled a nuanced hierarchy of isotherm fitting, with ELF > EL > MCL > JAMM in varying arsenic at a constant fluoride concentration, and ELF > JAMM > EL > MCL in varying fluoride at a constant arsenic concentrations. In addition, competitive studies divulged crucial insights into selective adsorption, as As(V) exhibits a pronounced adsorption selectivity over F on activated carbon. In

* Corresponding author.
** Corresponding author.
*** Corresponding author.
E-mail addresses: gautham.jeppu@manipal.edu (G. Jeppu), cr.girish@manipal.edu (C.R. Girish), murty.vytla@manipal.edu (V.R. Murty).

https://doi.org/10.1016/j.heliyon.2024.e31967
Received 17 January 2024; Received in revised form 24 May 2024; Accepted 24 May 2024
Available online 25 May 2024

essence, As(V) showed a more pronounced antagonistic behavior over F, whereas F exhibited a much lesser competitive behavior in the adsorption of arsenic.

Novelty statements

1. The research study presents a comprehensive exploration of the adsorption capabilities of activated carbon for the competitive removal of arsenic and fluoride in aqueous media.
2. Binary kinetic adsorption studies of arsenic and fluoride are limited , and were explored.
3. Comparison, modeling, and interpretation of competitive mechanisms are done for four multicomponent isotherms: Extended Langmuir, Extended Langmuir Freundlich, Modified Competitive Langmuir, and Jeppu Amrutha Manipal Multicomponent models.
4. The new multi-component isotherm model, i.e., Jeppu Amrutha Manipal Multicomponent (JAMM) isotherm developed in our previous research, was used for competitive adsorption simulation.

1. Introduction

Arsenic and fluoride in drinking water present a serious threat to the global population. These toxic elements have gained notoriety due to their widespread occurrence and detrimental effects on human health. These invisible pollutants in water have adversely impacted communities across various nations, leading to severe consequences. While anthropogenic activities and industrial discharge contribute to these toxic pollutants in water systems, it is also crucial to recognize that natural sources play a vital role. Arsenic and fluoride prevalence in wastewater and drinking water is a significant concern in numerous regions. For several decades, countries such as India [1], Mexico [2], Argentina [3], Australia [4], Pakistan [5], and Japan [6] have grappled with the co-occurrence of arsenic and fluoride in their groundwater sources. These pollutants seriously challenge public health and necessitate action to mitigate their effects [7].

When individuals consume arsenic-contaminated water, health risks are inevitable—consumption of arsenic results in a likelihood of developing cancer, liver disease, and a damaged nervous system. Additionally, individuals may experience complications such as hearing problems, loss of limb sensation, and digestive difficulties [8]. A minimal quantity of fluoride benefits teeth and bone development and dental health. The health problems associated with high fluoride levels include tooth decay and dental fluorosis. Furthermore, fluoride can cause skeletal fluorosis, which damages bones and joints. It has also been linked to thyroid problems, neurological issues, high blood pressure, myocardial damage, cardiac insufficiency, arteriosclerosis, arterial calcification, and heart failure [9]. According to reports, As(V) and F together have a more significant impact on the genetic integrity of cells than each substance alone. High concentrations of As(V) or F also harm children's growth and IQ. Therefore, it is crucial to eliminate these toxins from drinking water. The World Health Organization (WHO) has established limits for arsenic and fluoride in drinking water to address these pressing concerns. The recommended limit for arsenic is 0.01 mg/L, while for fluoride, it is 1.5 mg/L [10]. These guidelines serve as crucial benchmarks for governments and regulatory bodies in implementing measures to ensure safe drinking water for their

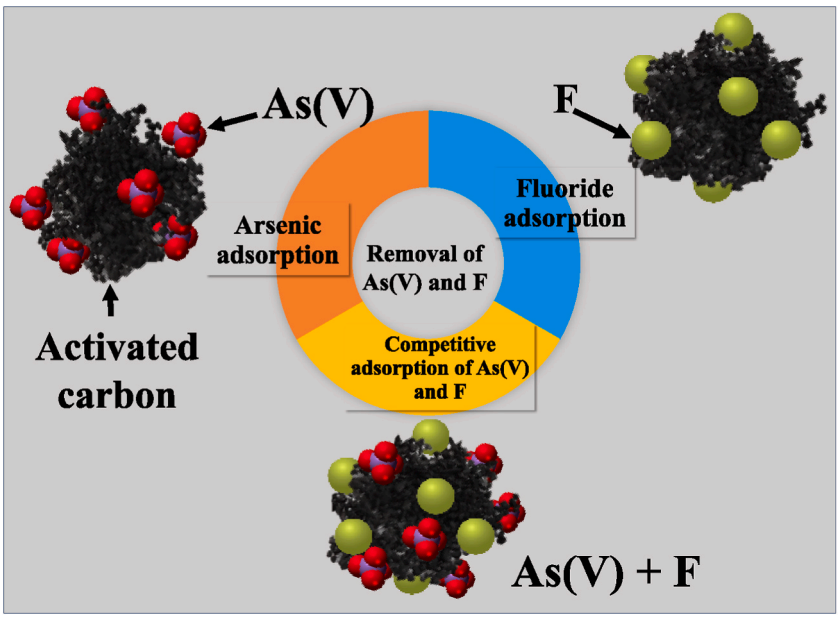

Fig. 1. Schematic representation of arsenic and fluoride adsorption on activated carbon in single and competitive adsorption systems.

populations [11].

Extensive research, as highlighted in the literature, has identified several successful adsorbents capable of removing arsenic and fluoride, such as activated carbon, novel iron, and iron-zirconium-modified activated carbon derived from Tectona grandis sawdust [12]. Various composite materials have been employed for this purpose, yielding promising outcomes. For instance, modified hydroxyapatite [13–16], aluminum alginate [17,18], activated alumina [8,19–21], zirconium oxide [12,22,23], chitosan composite [24,25], and impregnated lanthanum silica gel [26,27] have demonstrated adequate fluoride and arsenic removal capabilities [28]. Innovative approaches have also been explored, such as impregnating sawdust with ferric hydroxide and activated alumina for maximum sorption of arsenic and fluoride. Aluminum hydroxide/aluminum oxide nanoparticles have demonstrated efficient simultaneous removal of pollutants, with maximum Langmuir adsorption capacities for simultaneous removal of 0.833 mg/g and 2 mg/g for arsenic and fluoride, respectively [29]. Activated carbon fibers enhanced with zirconium (Zr-ACF) were made using a novel drop-coating technique which followed the pseudo-second-order adsorption kinetics model. Moreover, literature surveys have revealed that researchers have extensively utilized activated carbon derived from diverse materials to eliminate As(V) and F from aqueous solutions. Also, Fig. 1. Shows the schematic representation of arsenic and fluoride adsorption on activated carbon in single and competitive adsorption systems.

When two separate dangerous pollutants are consumed, they may effectively work independently, synergistically, or antagonistically to one another. The adverse effects of As(V) and F taken separately have been extensively researched, but their combined exposure has received little attention [3,30]. Despite the tremendous gravity of the situation, relatively little information is available on the populations simultaneously exposed to As(V) and F poisoning [11]. Addressing the issue of excess arsenic and fluoride in water systems requires a comprehensive approach encompassing both natural and anthropogenic sources. Additionally, mitigating the impact of natural sources through appropriate water management strategies and geological assessments can help minimize contamination [31]. The literature on the multi-component adsorption of arsenic and fluoride with modeling studies is limited, and the competitive adsorption of these contaminants is understudied. The analysis of competitive adsorption is imperative to devise effective strategies for water treatment and ensure the removal of arsenic and fluoride [32,33].

This study aims to comprehensively explore the use of activated carbon adsorbing the pernicious pollutants arsenic and fluoride in single and simultaneous systems. Furthermore, this study delves into various characterization techniques employed to evaluate the characteristic properties of activated carbon in pre-adsorbed and post-adsorbed stages. Additionally, it investigates the single sorption capabilities and other parameters using five non-linear regression analyses by Langmuir, Freundlich, Toth, Redlich Petersons, and modified Langmuir Freundlich models. We have compared the four nonlinear competitive isotherm models: the extended Langmuir, extended Langmuir Freundlich, modified competitive Langmuir, and Jeppu Amrutha Manipal multicomponent, which describes competitive mechanisms for simultaneous systems. Furthermore, the interpretation of the selectivity and competitive mechanisms behavior of binary As(V) and F adsorption systems has been made. Also, the normalized average percentage error (NAPE), root mean square error (RMSE), and correlation coefficient (R^2) statistical errors were analyzed to determine the fitness of predicted isotherms. Additionally, the investigation encompasses equilibrium studies and applying various adsorption isotherm models to elucidate the intricate sorption mechanisms.

2. Materials and methods

2.1. Chemical and reagents

0.416 g of $Na_2HAsO_4.7H_2O$ was used to prepare 100 ppm of arsenic solution. 0.221 g of NaF was used to prepare 100 ppm of the standard fluoride samples. NaOH or HCl was used to adjust the pH of the solution. The activated carbon (AC) purchased from Darco, USA, was granular and insoluble. The AC has been tested, and it has a selectivity range of up to 57, particle size 12–20 mesh, and high purity grades from Sigma Aldrich.

2.2. Characterization of activated carbon (AC)

The characterization of AC was carried out by Brunauer Emmett Teller (BET) apparatus, Fourier transform infrared spectroscopy (FTIR), X-ray Diffraction (XRD), Field Emission Scanning Electron Microscope (FESEM), and Energy Dispersive Spectroscopy (EDS). BET apparatus (Smart Instruments, Mumbai) gave the surface area and pore volume. The functional groups were identified by the FTIR (Thermo Scientific, USA) and the XRD (EMPyrean range, Malvern PANalytical, Netherlands), a non-destructive technique that recognized AC's crystal phases and structure. FESEM (FEI. Quanta 200, Thermofishcher, USA) and EDS (Irtracer 100, Shimadzu, USA) investigated the morphology, orientation, composition, and topography.

2.3. Adsorption kinetics and isotherms

The single and binary adsorption studies of As(V) and F ions onto AC were conducted in batch mode at 25 ± 2 °C.

In a typical procedure for single kinetic experiments, 250 mL of solute concentration was taken in 250 mL conical flasks, and 1.25 g of AC was added at pH value 5 ± 0.02. The flasks were kept in an incubator shaker at 250 rpm. The aliquots were taken at regular time intervals up to 4 days. Similarly, adsorption isotherm experiments were performed with different initial concentrations of 1–100 mg/L by adding 5 g/L of AC to 50–100 mL solution in 250 mL conical flasks with pH 5 ± 0.02 at 25 ± 2 °C for 48 h. Then, the solution was filtered by microfilters. A flame atomic absorption spectrophotometer (AAS) measured and detected the arsenic concentration and

quantified arsenic trace levels. A Thermo Orion Ion-Selective Fluoride meter (FM) advanced instrumentation ensured the robustness of experimental findings by gauging the fluoride concentration. The effect of pH on the adsorption capacity of AC was determined by adjusting the pH range of 3–11; initial concentrations were 10 mg/L for As(V) & F. Fig. 2. Shows the experimental flowchart of arsenic single adsorption system. Finally, the metal ion adsorption at equilibrium onto AC in aqueous solution was evaluated by the equation:

$$Q_e = \frac{(C_0 - C_e)\, V}{m} \quad \text{Eq. (1)}$$

where C_o is the initial concentration (mg/L), C_e is the final concentration (mg/L), V is the volume of aqueous solution (L), and m is the adsorbent dosage (g/L).

The operating conditions of the binary adsorption systems were prepared similarly to those of single adsorption systems. The kinetics and isotherm experiments were conducted in triplicates; the average standard deviation values were considered. The time-dependent pseudo-first-order, pseudo-second-order, Elovich, and intraparticle diffusion kinetic models were fitted for single and binary systems. Langmuir, Freundlich, modified Langmuir Freundlich, Toth, and Redlich Peterson isotherm models were modeled and simulated for single-component systems. Additionally, the competitive mechanisms of four multicomponent isotherms: extended Langmuir, extended Langmuir Freundlich, modified competitive Langmuir, and Jeppu Amrutha Manipal multicomponent were compared, modeled, and interpreted models.

2.4. Adsorption kinetics

1 The pseudo-first-order kinetic model

$$q_-(t) = q_-(e)\left(1 - e^{-k_L t}\right) \quad \text{Eq. (2)}$$

Where k_L (min^{-1}) is the coefficient of pseudo-first-order adsorption rate, q_e, and q_t are the ion adsorbed (mg/g) quantity at equilibrium and time t, respectively.

2 The pseudo-second-order kinetic model

$$q_t = \frac{k_2 q_e^2 t}{1 + k_2 q_e t} \quad \text{Eq. (3)}$$

Where k_2 is the pseudo-second-order rate constant (g/mg min), q_e and q_t are the quantity of ion adsorbed (mg/g) at equilibrium and time t, respectively.

3 The Elovich equation kinetics model

$$q_t = \frac{1}{b} ln\,(1 + abt) \quad \text{Eq. (4)}$$

Where q_t is the adsorbate concentration at any time, t, per weight of adsorbent (mg/g), a is the Elovich constant related to the initial adsorption rate (mg/g min), b is the Elovich constant related to the desorption rate (g/mg).

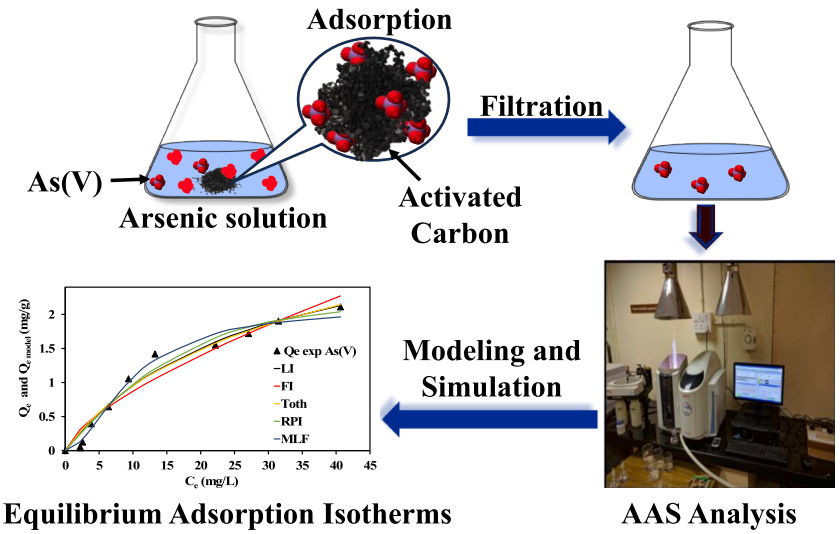

Fig. 2. Experimental flowchart of arsenic single adsorption system.

4 The intraparticle diffusion model

$$q_t = k_i t^{0.5} + C \quad \text{Eq. (5)}$$

Where k_i is the intraparticle diffusion rate constant (g mg^{-1} $min^{-1/2}$), and C is the surface adsorption.

2.5. Mono component adsorption isotherms

1 Langmuir isotherm model (LI)

$$Q_e = Q_m \frac{k_L C_e}{1 + k_L C_e} \quad \text{Eq. (6)}$$

Where C_e is the adsorbate concentration at equilibrium (mg/L), Q_e is the equilibrium adsorption capacity of adsorbents (mg/g), Q_m is the maximum adsorption capacity (mg/g), k_L is the Langmuir constant expressed as L/mg, and C_o is the initial concentration of the solution expressed as mg/L. The adsorbent sites will have the same energy to attract the adsorbates. It assumes the formation of a monolayer, homogenous surface, and no interactions between the adsorbates [34].

2 Freundlich Isotherm model (FI)

$$Q_e = k_F C_e^{1/n} \quad \text{Eq. (7)}$$

k_F is adsorption capacity (L/mg), and 1/n is adsorption intensity. It indicates relative energy distribution and the adsorbate sites' heterogeneity. The value of 1/n indicates the favorability of the adsorption, i.e., if 1/n is greater than 0, or $0 < 1/n < 1$, then adsorption is favorable, and when $1/n = 1$, adsorption does not occur. A reversible multilayer on the heterogeneous surface is established. The distribution of components depends on the time and energy of the sites ensured [35].

3 Redlich Peterson Isotherm model (RPI)

$$q_e = \frac{k_{RP}\, C_e}{1 + \alpha_{RP}\, C_e^{\beta}} \quad \text{Eq. (8)}$$

k_{RP} and α_{RP} are the Redlich-Peterson isotherm model constants, and β is the exponent of the Redlich-Peterson isotherm, which lies between 0 and 1. It obeys Langmuir and Freundlich models, but it is not monolayer adsorption. It pertains to homogeneous or heterogeneous surfaces [36].

4 Toth Isotherm model

$$q_e = \frac{k_T\, C_e}{(\alpha_T + C_e)^{\frac{1}{\tau}}} \quad \text{Eq. (9)}$$

k_T and α_T are the Toth isotherm model constants, and τ is the exponent of the Toth isotherm, which lies between 0 and 1. It has the vital function of operating both in low and high concentrations. Langmuir model is modified to diminish the errors between experimental and predicted data [37].

5 Modified Langmuir Freundlich Isotherm model (MLF)

$$Q_e = Q_m \frac{[C_e k_a]^n}{1 + [C_e k_a]^n} \quad \text{Eq. (10)}$$

Q_m is the maximum adsorption capacity of the system (mg/g), C_e is the aqueous phase concentration at equilibrium (mg/L), k_a is the affinity constant for adsorption (L/mg), and n is the index of heterogeneity. In the above equation, the affinity constant (k_a) value can be varied for pH-dependent sorption effects. The uniqueness of this isotherm is its pH dependency on adsorption systems. The essential experimental condition required to apply this isotherm model in a system is pH [38].

2.6. Multicomponent adsorption isotherms

An extension of single-component adsorption isotherms is multicomponent adsorption isotherms. The multicomponent isotherm was derived based on the single adsorption isotherm. This work simulated experimental data using five multicomponent adsorption isotherms described below.

1 Extended Langmuir Isotherm/Non-Modified Langmuir Isotherm model (EL)

$$Q_{e,i} = Q_{m,i}\frac{K_{L,i}c_{e,i}}{1+\sum_{j=1}^{N}K_{L,i}c_{e,i}} \quad \text{Eq. (11)}$$

Where $Q_{e,i}$ and $Q_{e,j}$ is the equilibrium adsorption capacity for components i and j (mg/g), $Q_{m,i}$ and $Q_{m,j}$ is the maximum adsorption capacity for components i and j (mg/g), $K_{L,i}$ and $K_{L,j}$ is the Langmuir constant for components i and j (L/mg) and $c_{e,i}$ and $c_{e,j}$ is the equilibrium concentration for components i and j (mg/L), respectively. N is the number of components, and '*j*' takes from 1 to N. The active sites on the adsorbent are assumed to be uniform and to have the same energy in this model. Pollutant molecules also adhere to the active sites due to the adsorbates' non-interacting action. The drawback of this approach is that the values of the isotherm parameters for other adsorption systems might be drastically different [39].

2 Extended Langmuir-Freundlich Isotherm Model (ELF)

$$Q_{e,i} = Q_{m,i}\frac{K_{LF,i}c_{e,i}^{\left(1/n_i\right)}}{\sum_{j=1}^{N}K_{LF,i}c_{e,i}^{\left(1/n_i\right)}} \quad \text{Eq. (12)}$$

Where $Q_{e,i}$ and $Q_{e,j}$ is the equilibrium adsorption capacity for components i and j (mg/g), $Q_{m,i}$ and $Q_{m,j}$ is the maximum adsorption capacity for components i and j (mg/g), $K_{L,i}$ and $K_{L,j}$ is the Langmuir constant for components i and j (L/mg), $c_{e,i}$ and $c_{e,j}$ is the equilibrium concentration for components i and j (mg/L) and n_i and n_j is the adsorption intensity for components i and j (mg/g), respectively. This isotherm model is the combination of Langmuir and Freundlich's isotherm models. At n, the heterogeneity index value reduces to one; isotherm behaves as the Extended Langmuir isotherm model [40].

3 Modified Competitive Langmuir Isotherm Model (MCL)

$$Q_{e,i} = Q_{m,i}\frac{K_{L,i}\left(c_{e,i}/\eta_{L,i}\right)}{1+\sum_{j=1}^{N}K_{L,j}\left(c_{i,j}/\eta_{L,j}\right)} \quad \text{Eq. (13)}$$

Where $Q_{e,i}$ and $Q_{e,j}$ is the equilibrium adsorption capacity for components i and j (mg/g), $Q_{m,i}$ and $Q_{m,j}$ is the maximum adsorption capacity for components i and j (mg/g), $K_{L,i}$ and $K_{L,j}$ is the Langmuir constant for components i and j (L/mg), $c_{e,i}$ and $c_{e,j}$ is the equilibrium concentration for components i and j (mg/L), and η_i and η_j is the interaction factor for components i and j (mg/g), respectively. When η, the interaction factor value reduces to one, MCL behaves as the extended Langmuir isotherm model [41].

4 Jeppu Amrutha Manipal Multicomponent Isotherm Model (JAMM)

$$Q_{e,i} = Q_{m,i}\frac{\Phi_i\, x_i\, \left(K_{L,i}\, C_{e,i}\, a_i\right)^{n_i}}{1+\sum_{j=1}^{N}\left(K_{L,i}\, C_{e,i}\, a_i\right)^{n_i}} \quad \text{Eq. (14)}$$

Where $Q_{e,i}$ and $Q_{e,j}$ is the equilibrium adsorption capacity for components i and j (mg/g), $Q_{m,i}$ and $Q_{m,j}$ is the maximum adsorption capacity for components i and j (mg/g), $K_{L,i}$ and $K_{L,j}$ is the Langmuir constant for components i and j (L/mg), $c_{e,i}$ and $c_{e,j}$ is the equilibrium concentration for components i and j (mg/L), n_i and n_j is the heterogeneity index for components i and j (mg/g), Φ_i and Φ_j is the interaction coefficient for components i and j (mg/g), a_i and a_j is the affinity factor for components i and j (mg/g) and x_i and x_j is the mole fractions for components i and j (mg/g), respectively [42].

2.7. Analysis of statistical errors

The least-square fit assesses the model parameters and helps to compare the error distribution. The sum of squared errors was minimized while calculating the model parameter, and also the average percentage error between the experimental and predicted values was determined. The correlation coefficient (R^2) value determines the model's acceptability. To this purpose, the root mean square error (RMSE), the sum of squared error (SSE), and normalized average percentage error (NAPE) [42] error functions were utilized to validate the fitness of the models examined in the current investigations [35].

$$SSE = \sum_{i=1}^{N}\left(Q_{exp} - Q_{cal}\right)^2 \quad \text{Eq. (15)}$$

$$RMSE = \sqrt{\frac{\sum_{i=1}\left(Q_{exp} - Q_{cal}\right)^2}{N}} \quad \text{Eq. (16)}$$

$$NAPE = \sum_{i=1}^{N} \left\{ \frac{Q_{exp} - Q_{cal}}{Q_{e,max}} \right\} \frac{100}{N} \quad \text{Eq. (17)}$$

Q_{exp} is the experimental data, Q_{cal} is the predicted data, $Q_{e,max}$ is the maximum experimental data, and N is the number of experimental data points. The lower the values of SSE and RMSE and the greater the R^2, the more suitable the model.

2.8. Desorption and regeneration of activated carbon

To understand the significance of desorption studies in assessing the activated carbon's durability, quality, operational expenses, maintenance, and reusability. Henceforth, both adsorption and desorption investigation studies were performed. After the adsorption experiments by As(V) and F, eluting reagents like NaOH, HCl, and distilled water were employed [43]. The desorption percentage of AC was gauged after each desorption cycle. The regeneration studies were carried out for the adsorbed AC utilized in single and binary adsorption of As(V) and F.

After each consecutive regeneration cycle, the desorption efficiency was evaluated. Therefore, desorption efficiency is given by,

$$DE = \frac{C_o - C_e}{C_o} X\ 100 \quad \text{Eq. (18)}$$

Where, c_o and c_e are each cycle's initial and equilibrium concentrations of As(V) and F (mg/L) in the adsorbent.

3. Results and discussion

3.1. Characterization of activated carbon

3.1.1. Surface area and pore volume

The Brunauer Emmett Teller (BET) apparatus determined the surface area and pore volume of activated carbon. The surface area depicted the availability of active sites on AC. In this study, the surface area was 568.14 m^2/g, and the pore volume was 0.4507 cc/g. The average pore size of the AC was calculated to be 3.1731 nm, indicating that it falls within the mesopores range. Table 1 shows the physicochemical properties of AC. Previous works have obtained similar results [44–48]. As the relative density of AC was greater than that of water, AC was denser and with less moisture content.

3.1.2. Field Emission Scanning Electron Microscopy (FESEM)

The Field Emission Scanning Electron Microscopy (FESEM) technique was employed to determine the morphology and orientation of AC. Fig. 3(a) displays the FESEM images of plain AC magnified at 25kX. The images revealed a uniform and porous surface; previous literature reported similar results [52,53]. The electron mapping confirms the presence of arsenic and fluoride adsorbed on the AC after adsorption, depicting the existence in Fig. 3(a).

3.1.3. Energy Dispersive X-ray Spectroscopy (EDS)

The Energy Dispersive X-ray Spectroscopy (EDS) technique provided compositional and topographic information. The EDS spectrum in Fig. 3(b) confirmed the presence of essential elements such as carbon and oxygen in the AC. The intense spectrum was observed within the 0–1 keV range, and the peaks in the EDS spectrum indicated the presence of carbon. The atomic percentage of carbon was found to be 33.33 %, while oxygen accounted for 66.67 % of the AC composition. EDS depicted the atomic percentage of arsenic and fluoride after adsorption. Similar results were obtained in previous studies as well [54–57].

3.1.4. Fourier transform infrared spectroscopy (FTIR)

The FTIR spectra in Fig. 3(c) illustrates FTIR (before and after adsorption of arsenic), (d) FTIR (before and after adsorption of fluoride), (e) FTIR (before and after adsorption of arsenic and fluoride). The peak was observed at 771.47 cm^{-1}, 1040.99 cm^{-1},

Table 1
The physicochemical properties of AC.

No	Properties of AC	Specifications
1	Appearance: Form	Granular (12–20 mesh)
2	Autoignition temperature	842 F
3	Moisture content	≤12 %
4	Particle size	12–20 mesh
5	Surface area	568.14 m^2/g
6	Pore volume	0.4507 cc/g
7	Selectivity	~57
8	Melting point/Freezing point	3.550 C - lit
9	Relative density	1.8–2.1 g/cc
10	Water solubility	Insoluble

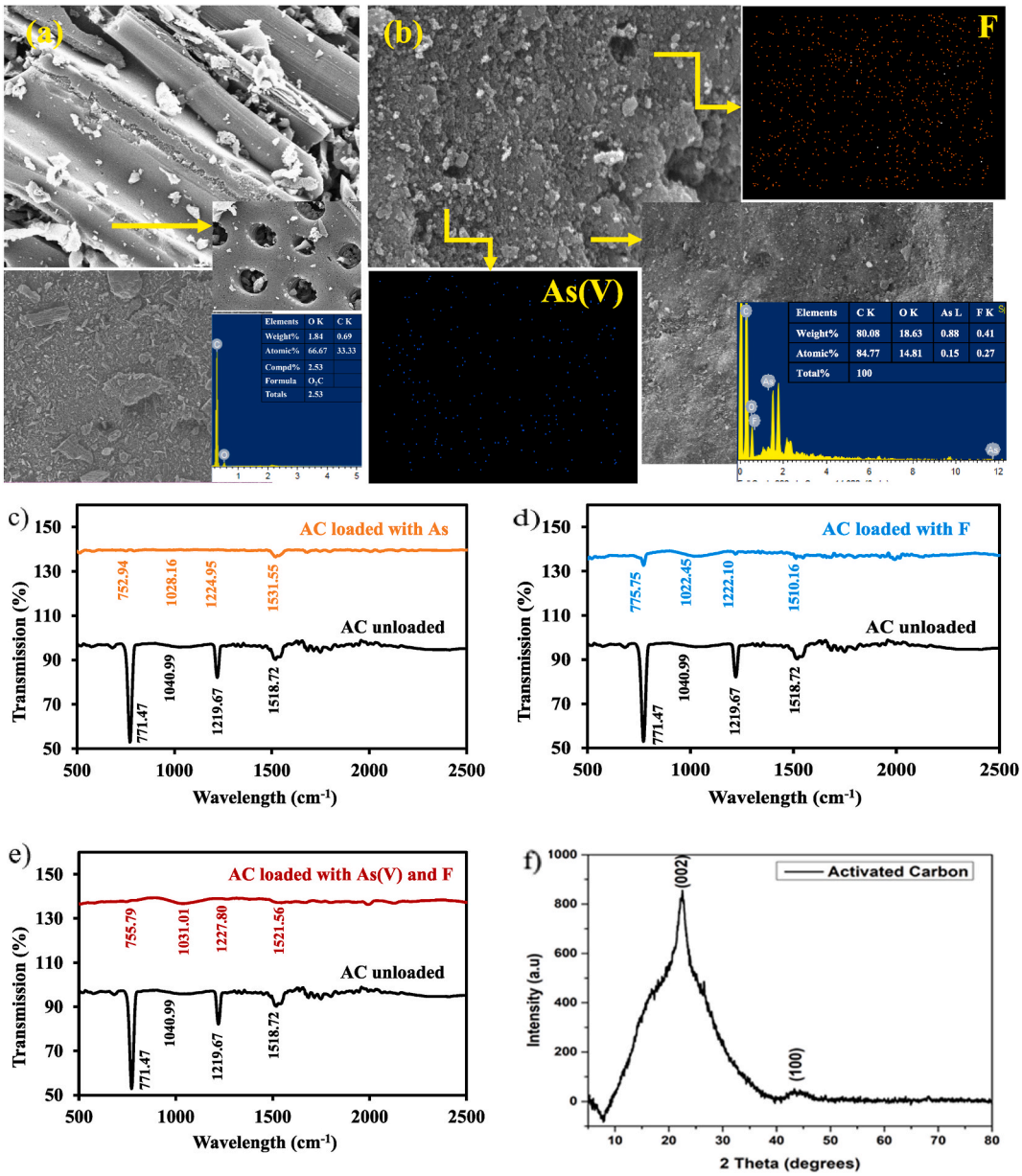

Fig. 3. (a) FESEM and EDS (before) and (b) FESEM and EDS (after adsorption), (c) FTIR (before and after adsorption of arsenic), (d) FTIR (before and after adsorption of fluoride), (e) FTIR (before and after adsorption of arsenic and fluoride), (f) XRD analysis of activated carbon.

Table 2
The FTIR spectral properties of activated carbon.

Peak	Activated carbon (Frequency range, cm^{-1})							Assignment	Ref.
	Unloaded	Loaded							
	AC	As(V)	difference	F	difference	As(V) and F	difference		
1	771.47	752.94	+18.53	775.75	−4.28	755.79	+15.68	C–H stretch, Alkenes	[49–51]
2	1040.99	1028.16	+12.83	1022.45	+18.54	1031.01	+9.89	Skeletal C–C vibrations	
3	1219.67	1224.95	−5.28	1222.10	−2.53	1227.80	−8.13	Aromatic C–H in-plane blend	
4	1518.72	1531.55	−12.83	1510.16	+8.56	1521.56	−2.84	C═C–C Aromatic ring stretch	

1219.67 $cm^{-1,}$ and 1518.72 cm^{-1}. These were the possible sites for the adsorption. The band spectra were found in the fingerprint region, i.e., 400 to 1500 frequencies. However, the FTIR results showed that these bands' intensity differences exceeded after arsenic and fluoride adsorption. The peaks at different bands disappeared after the adsorption of the pollutant, as shown in Fig. 3. The difference in the peaks and assignments is noted in Table 2.

4.1.5. X-ray Diffraction (XRD)

The X-ray Diffraction (XRD) pattern exhibited two major diffraction peaks at $2\theta = 21.92°$ and 44.05°, corresponding to the (002) and (100) planes, respectively, as in Fig. 3(f). These peaks align well with the Joint Committee on Powder Diffraction Standards (JCPDS) file 41–1487, indicating that the AC possesses an amorphous and graphitic structure. Previous studies have also been reported this observation [58,59]. The average particle size of AC was 1.102 nm, determined using the Scherrer equation, considering the peak locations. Fig. 3(f) shows XRD pattern for activated carbon.

4. Adsorption study in a single and simultaneous system

4.1. Percentage removal

In the single and binary systems, adsorption experiments were performed for As(V) and F using AC. The experiments were conducted with a volume (V) of 50 mL, pH value of 5, a dosage of 5 g/L, temperature (T) set at 25 °C, initial concentration (C_o) of 100 mg/L, and agitation speed of 150 rpm. The influence of contact time on the percentage removal of arsenic and fluoride in single and binary component systems is shown in Fig. 4(a and b). In a single-component system, the percentage removal of arsenic increased with increasing contact time until 48 h, which further varied slightly. Also, it marginally increased in the binary component system with increasing contact time up to 30 h. Similarly, the percentage removal of fluoride increased with the increasing contact time till 30 h, after which the removal continued until saturation, and in the binary component system, removal increased with the increasing contact time till 40 h, after which the removal of fluoride slightly varied with the increasing contact time.

The experiment initially observed the highest reduction of arsenic and fluoride levels. This can be attributed to the abundance of vacant sites on the adsorbent surface during the early stages of the experiment, facilitating rapid removal. As time progressed, As(V) and F concentrations steadily declined [60,61]. The decline can be attributed to a gradual decrease in the driving force propelling the adsorption. Meanwhile, the agitation speed remained constant, maintaining a consistent interaction level between A(V), F, and AC, leading to an equilibrium state. Ultimately, the equilibrium state emphasized the importance of considering the saturation point [62,63]. As a result, the adsorption rate during this period was more noticeable. Therefore, the optimal contact time for arsenic and fluoride adsorption was 48 h in both single-component and binary-component systems. In the single-component system, the study achieved a percentage removal of 93.56 % for arsenic and 72 % for fluoride.

Similarly, in the binary-component system, the percentage removal of As(V) was 71.91 %, while fluoride was removed at a rate of 90 %. This reduction was due to the competitive behavior of fluoride or vice versa. Though ions try to reach the AC's active sites, competition arises in the binary systems [64]. Additionally, the affinity of AC towards arsenic and fluoride differs, leading to a variation in the removal percentage in binary adsorption. AC's chemical composition and surface characteristics determined its preference to adsorb certain pollutants [65–67].

4.2. Effects of adsorbent dosage

For As(V) & F, the single and binary batch adsorption experiments were conducted at specific conditions: dosage ranging from 1 to 10 g/L, temperature (T) of 25 °C, initial concentration (C_o) of 100 mg/L, and agitation speed of 150 rpm for 48 h. Fig. 5(a and b) illustrates the impact of adsorbent dosage on removing arsenic and fluoride in single and binary-component systems.

Evidently, the adsorption rate was promisingly elevated with higher AC dosage. However, as the dosage increased, it was attributed to increased active sites and distribution coefficients, which promote higher interactions between the adsorbent and adsorbate.

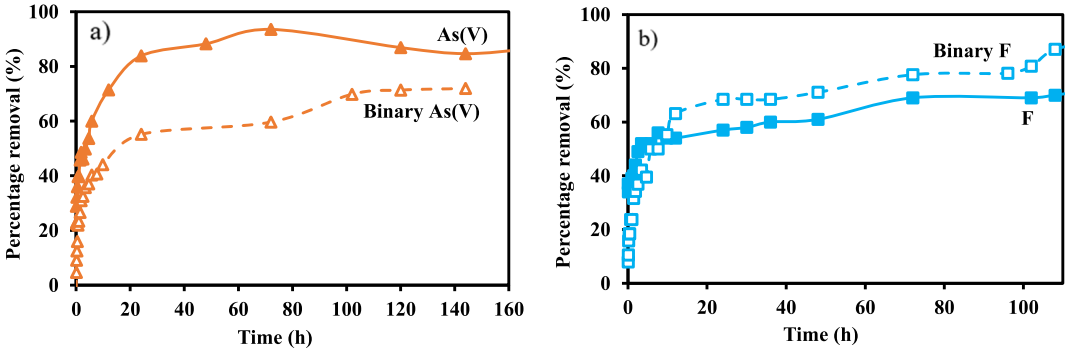

Fig. 4. Influence of contact time on percentage removal of a) arsenic and b) fluoride in single and binary component systems.

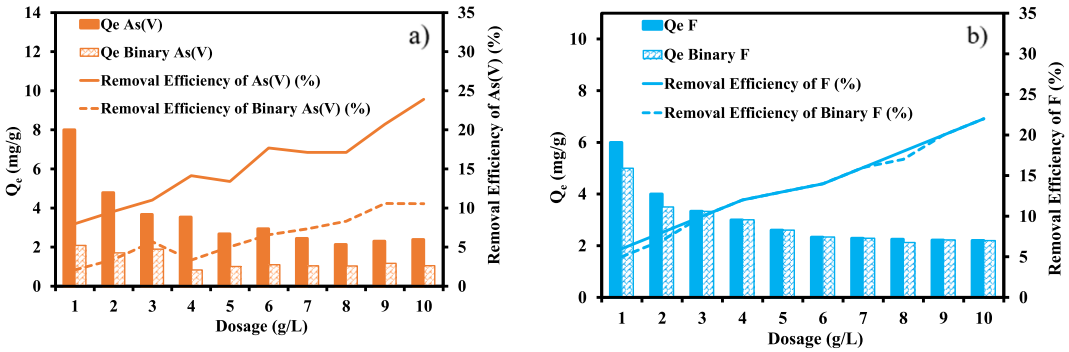

Fig. 5. Influence of adsorbent dosage on removal of a) arsenic and b) fluoride in single and binary component systems.

Consequently, the removal efficiency was also boosted with increased AC dosage. In both cases, the simultaneous removal efficiency was relatively less than the removal efficiency of a single system. This was an expected result as in previous works of literature [68,69]. As(V) sorption was affected more significantly than a single system in the presence of F. In contrast, F sorption was reduced gradually, but the removal was less significant in the presence of As(V). Moreover, based on the results obtained from the experiments of single and binary systems, the optimal adsorbent dosage for As(V) and F was taken as 5 g/L.

4.3. *Effect of pH and the point of zero charge (pH_{zpc})*

By using 50 ml of a 0.1 M NaCl solution, the point of zero charge (pH_{zpc}) of AC was ascertained. The pH was maintained between 3 and 11 by adding 0.1 N HCl and 0.1 N NaOH. After adding the AC to the mixture, the pH of the mix was assessed after 24 h. The pH_{zpc} value was determined by the plot ΔpH versus initial pH. The difference between the initial and final pH gave the pH_{zpc} [70,71].

From Fig. 6, it can be depicted that AC's zeta potential changes. The AC exhibited the point of zero charge (pH_{zpc}) at approximately pH 6.8. The surface charge of the material can be determined by the zeta potential [72]. The results showed that the surface of AC was positively charged if the pH of the solution was less than pH_{zpc}, zero charge if the pH of the solution was equal to $pH_{zpc,}$ and negatively charged if the solution's pH was higher than pH_{zpc}. However, similar outcomes were seen in earlier studies [56,73].

Fig. 7(a and b) shows that As(V) and F adsorption rise as pH lowers. The pH of the solution significantly affected the speciation of As (V) and F ions, influencing the reactions and other chemical forms [74]. The protonation and deprotonation of species were the impact of pH. At neutral pH, the primary dihydrogen arsenate, the chemical equilibrium is represented in Eq (19). Hence, the dominant species was $H_2AsO_4^-$, resulting in a negative charge and loss of one H^+ ion. At low pH (<7), in acidic conditions, protonation increases as H^+ ions increase, achieving more protonated species (Eq. (20)), resulting in more positively charged ions [75]. At pH > 7, OH^- ions were relatively high in primary conditions. The OH^- ions react with $H_2AsO_4^-$, leading to negatively charged species (Eq. (21)). Along with the charge of arsenate, the surface charge of AC at specific pH also varied the affinities and adsorption behavior [17]. At pH 3, adsorption was at its highest; However, as pH increased, adsorption decreased.

$$H_2AsO_4^- \rightleftharpoons H^+ + HAsO_4^{2-} \quad \text{Eq (19)}$$

$$H_2AsO_4^- + H^+ \rightleftharpoons H_3AsO_4 \quad \text{Eq (20)}$$

$$H_2AsO_4^- + OH^- \rightleftharpoons HAsO_4^{2-} + H_2O \quad \text{Eq (21)}$$

$$HF + H^+ \rightleftharpoons F^- \quad \text{Eq (22)}$$

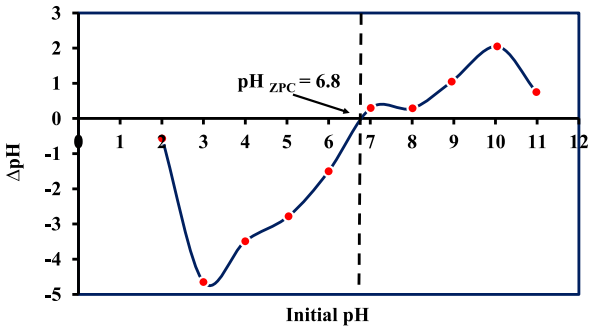

Fig. 6. Determination of point of zero charges using activated carbon as adsorbent (V = 50 mL, t = 25 °C, pH = 3 to 11, Dosage = 5 g/L, C_o = 0.1 M NaCl at 150 rpm for 24 h).

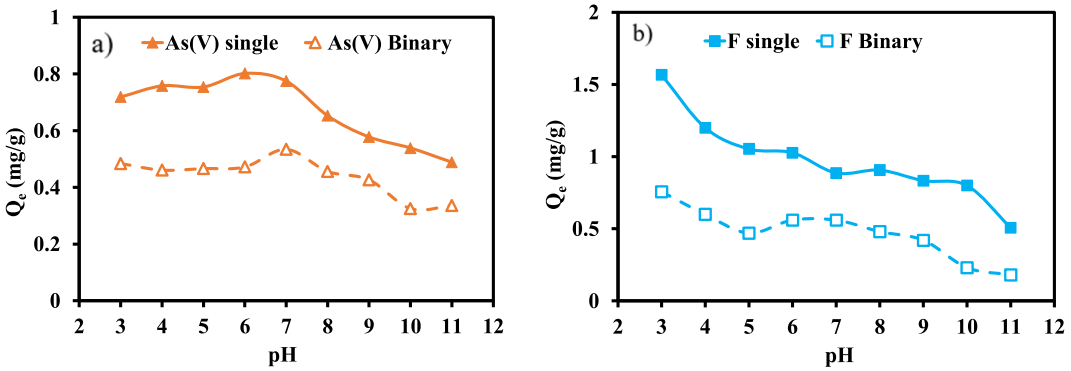

Fig. 7. Effect of pH on adsorption of a) As(V) and b) F for the single and binary system (V = 50 mL, t = 25 °C, pH = 3 to 11, Dosage = 5 g/L, C_o = 10 mg/L at 150 rpm using activated carbon as adsorbent).

$$F^- + H^+ \rightleftharpoons HF \quad \text{Eq (23)}$$

$$HF + OH^- \rightleftharpoons F^- + H_2O \quad \text{Eq (24)}$$

While, in the case of fluoride, at pH = 7, sodium fluoride exists prominently in fluoride ion (F^-) as in Eq. (22). The protonation occurs when the pH < 7 increases in the formation of HF in acidic conditions (Eq. (23)). In primary conditions, pH > 7, OH^- ions react with HF forming fluoride ions (Eq. (22)). It was perceived that negatively charged fluoride have more affinity towards positively charged AC [12]. Similarly, the maximum adsorption was attained at pH 3 according to experimental findings for F adsorption. The As (V) and F were adsorbed at a lower rate when the pH of the solution exceeded. As pH rises, there might be less availability of positively charged AC surface for negatively charged fluoride ions and competition between the hydroxyl and fluoride ions. As(V) and F exhibit a similar considerable adsorption reduction behavior with increasing pH in a binary system, as in Fig. 7(a and b) [76].

4.4. Adsorption kinetics study

The results of kinetic adsorption studies with the function of contact time for As(V) and F in a single component system are given in Fig. 8(a and b). The experimental conditions for the kinetics where the initial concentration was C_o = 10 ppm, the volume of solution taken was 250 mL, pH = 5, the dosage of AC taken was 5 g/L, agitation = 200 rpm, and temperature = 25 °C. It shows that As(V) adsorption on AC was more than that of fluoride in a single-component system. Initially, the adsorption was slow, but the adsorption process extended to 24 h, reaching equilibrium.

The parameters of adsorption kinetics are given in Table 3 for a single-component system of As(V) and F; also, the value of q_e of arsenic and fluoride was 1.53 mg/g and 1.20 mg/g. The linear relationship between log (q_e-q_t) vs. t for As(V) and F did not fit well, as given in Fig. S1 in supplementary data, indicating that adsorption involves more than one mechanism, and the q_e value was the same as q_t. Likewise, the relationship between ln(t) vs. t for As(V) and F was not linear, as in Fig. S2 in supplementary data, and the q_e value was similar to q_t [77,78].

The coefficient of determination (R^2) was closer to 1 in a pseudo-second-order reaction [79]. The t/q_t vs. t values showed linearity for the pseudo-second-order equation, as shown in Fig. 9(a and b). Henceforth, the adsorption process attributes pseudo-second-order reaction. The pseudo-second-order equation approximates the kinetics of specific chemical reactions, particularly those involving adsorption processes. It assumes a chemisorption mechanism, where the adsorbate species interacts with the surface through chemical

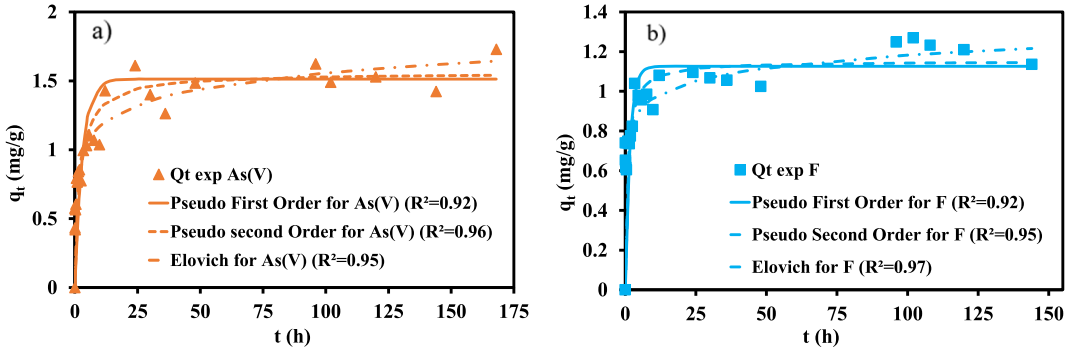

Fig. 8. Kinetic adsorption model fit of a) As(V) and b) F in a single component system.

Table 3
The parameters of a kinetic model of As(V) and F in the single adsorption system by AC.

Kinetic Model	Parameters	As(V)	F
Pseudo-First-Order Kinetic Model	q_t (mg/g)	1.48	1.13
	k (min^{-1})	0.005	0.009
	R^2	0.92	0.92
Pseudo-Second-Order Kinetic Model	q_t (mg/g)	1.55	1.15
	k_2 (g/(mg.min))	0.006	0.017
	R^2	0.96	0.95
Intra-particle Diffusion Kinetic Model	k_i (mg/g.$min^{0.5}$)	0.009	0.005
	C_i	0.83	0.81
	R^2	0.95	0.95
Elovich Kinetic Model	α (g/(mg.min))	0.34	4.47
	β (g/mg)	6.13	10.63
	R^2	0.95	0.97

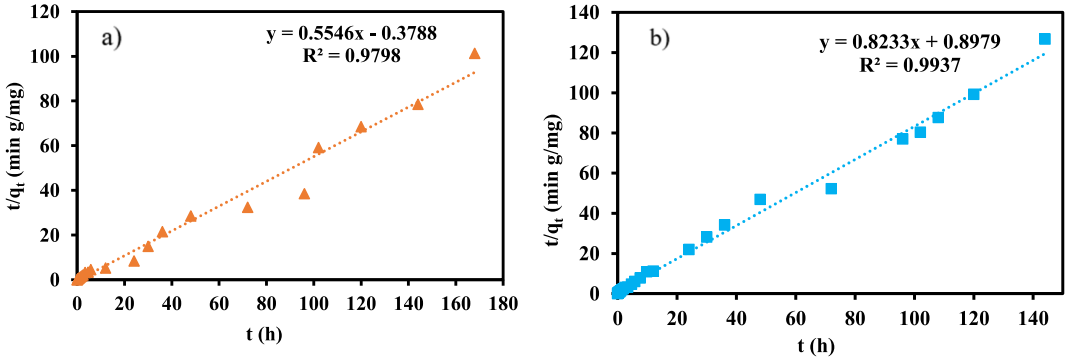

Fig. 9. Test of the pseudo-second-order equation for a) As(V) and b) F in the single component system.

bonds [80,81]. Additionally, it assumes that the rate of site occupation is proportional to the square of the number of unoccupied sites, which is a characteristic of specific adsorption processes. In the pseudo-second-order equation, the rate constant is usually called k_2. A higher rate constant indicates a faster reaction speed, which means the reaction proceeds more quickly [79,82].

In this study, the reaction rate constant k_2 and q_t of As(V) was 0.006 and 1.55 mg/g & for F was 0.017 and 1.15 mg/g, as shown in Table 3. Therefore, the rate of the chemical reaction was more rapid in the case of fluoride adsorption than in arsenic adsorption. The pseudo-second-order model fitted the adsorption kinetics much better than the pseudo-first-order and Elovich models for both adsorbates [83,84]. Although the pseudo-second-order model assumes that the rate-determining step is chemical adsorption, it is always monolayer adsorption, and the q_e value was the same as q_t. Thus, the concentration may indicate physical adsorption contributing at higher concentrations, i.e., the formation of more than one layer on the adsorbent surface. However, it also describes the complex reaction mechanisms and multiple steps involved in chemical reactions [85].

The intraparticle diffusion model includes all adsorption steps, such as external film (boundary layer) diffusion, pollutants reaching the pores, internal particle diffusion, rate-limiting step, and adsorption equilibrium. Initially, the As(V) and F molecules in solution contacted the external surface of AC [77,86]. The parameter C (constant) in the equation gives the thickness of the boundary layer. The more significant the C value, the greater the boundary layer. Amongst As(V) and F, As(V) has a more significant boundary layer than F [61]. As(V) and F molecules diffused into the pores of AC and moved gradually more profoundly into the pores. Factors like concentrations, pore size, and pollutant size influence the rate-limiting step. The slowest step controls the overall rate of adsorption. Of the five mentioned steps, the fifth step is assumed to be rapid, and thus, the slowest step would be either film diffusion or pore diffusion. However, intra-particle and external transport mechanisms might distribute the controlling step. Therefore, the intraparticle diffusion model comprehensively determines the adsorption process, as depicted in Fig. S4 in supplementary data [87].

The results of kinetic adsorption studies with the function of contact time for As(V) and F in binary component systems are given in Fig. S3 in supplementary data. The kinetic adsorption experiments of As(V) in a binary component system were conducted at V = 250 mL, pH = 5, Dosage = 5 g/L, T = 25 °C, C_o = 10 mg/L of As(V) and F at 200 rpm using AC as adsorbent. As(V) significantly adsorbed more than fluoride on AC. Initially, the adsorption was slow, but then the adsorption process increased to 24 h, reaching equilibrium [88,89]. The coexistence of As(V) and F significantly influenced adsorption kinetics, with notable alterations in the rate and the extent of adsorption at equilibrium time [61,90]. Competitiveness initiates interactions' complexity, directly impacting affinity and overall adsorption. Henceforth, simultaneous removal involves the interaction between the As(V) and F to reach the AC surface, and between the molecules of As(V) and F. As(V) and F coexistence underscores the complexity and highlights the need for precise removal strategies.

4.5. Single adsorption isotherms study

The adsorption isotherm experiments were performed with different initial concentrations of 1–100 mg/L by adding 5 g/L of AC to 50–100 mL solution in 250 mL conical flasks with pH 5 ± 0.02 at 25 ± 2 °C for 48 h. Isotherm adsorption was studied to determine the maximum adsorption capacity of AC for As(V) and F. The equilibrium data of As(V) & F were better depicted by single isotherm models like Langmuir (Eq. (6)), Freundlich (Eq. (7)), Toth (Eq. (8)), Redlich Peterson (RP) (Eq. (9)) and modified Langmuir Freundlich (MLF) (Eq. (10)) isotherm models for single-component systems as in Fig. 10(a–e). The results shows that adsorption capacity of AC was more significant for As(V) than fluoride.

Compared to other adsorbents, AC has a substantially superior adsorption capacity. AC was a potential material for extracting As(V) and F from aqueous solution [82,91]. The separation factor can determine the nature of adsorption. It is expressed as

$$R_L = \frac{1}{1 + K_L C_o} \quad \text{Eq. (25)}$$

C_o is the initial concentration, and K_L is the solution's isotherm constant of As(V) and F. The values of R_L signify the type of isotherms. It is unfavorable adsorption if the R_L values exceed 1 ($R_L > 1$). If the values lie between 0 and 1, it's favorable adsorption; if $R_L = 0$, adsorption is irreversible. Hence, R_L values of As(V) and F onto AC lie between 0 and 1, as shown in Table 4, indicating favorable adsorption [79]. The experimental adsorption equilibrium data of As(V) and F in single-component systems on AC were analyzed. The calculated coefficient of determination (R^2) and root mean square errors (RMSE) of five single isotherm models are represented in Table 4.

Table 4 shows the Langmuir isotherm with an adsorption capacity of AC of 3.58 and 2.32 mg/g for As(V) and F, respectively. The

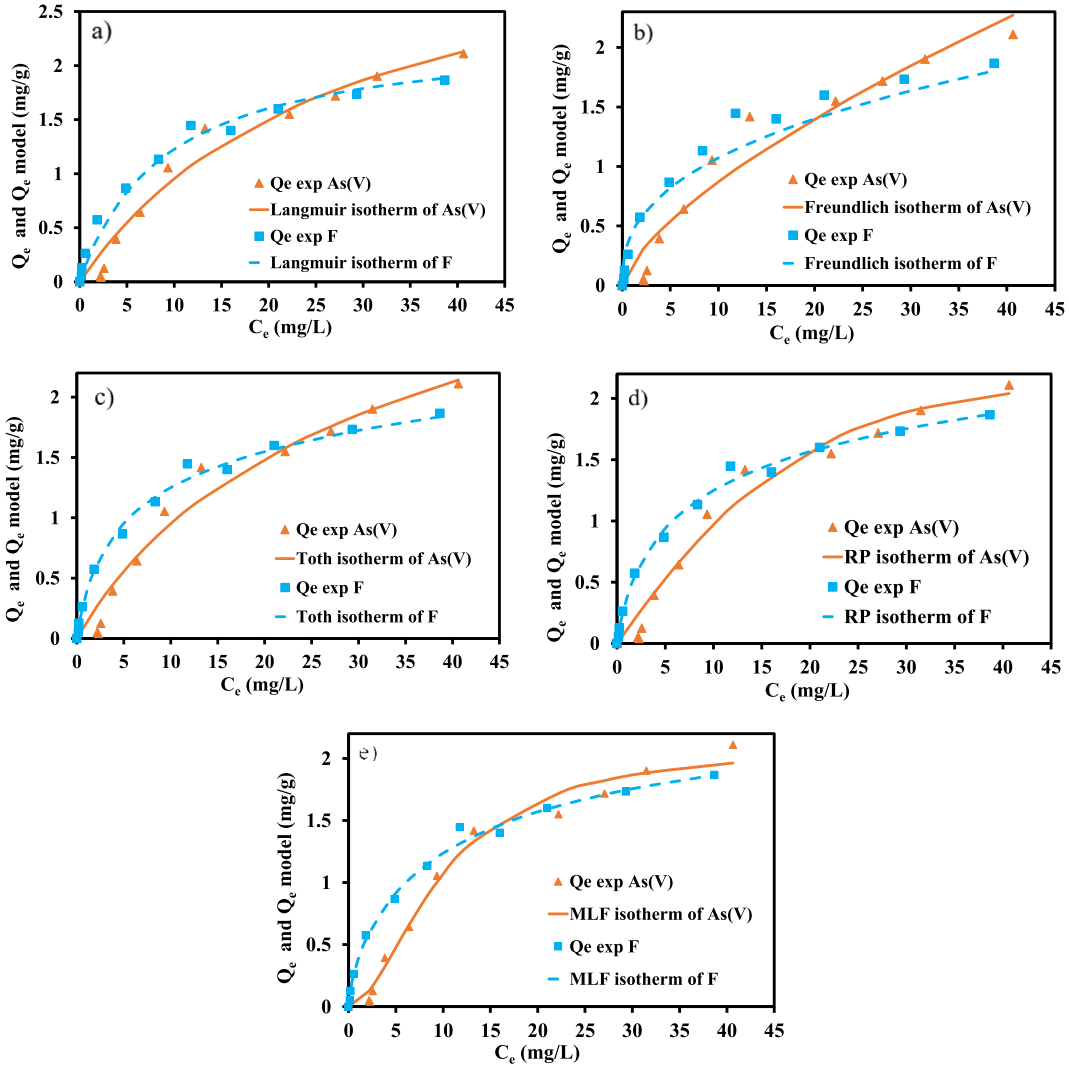

Fig. 10. a) Langmuir b) Freundlich c) Toth d) Redlich-Peterson e) modified Langmuir Freundlich isotherm model fit of As(V) and F.

Table 4
Equilibrium adsorption isotherm parameters and errors of the single component system for As(V) and F by activated carbon.

Isotherm Model	Component	Parameters	R_L	R^2	NAPE (%)	RMSE
Two-parameter Langmuir Isotherm Model (LI)	As	$k_L = 0.036$ L/mg $Q_m = 3.58\ mg/g$	0.74	0.97	5.28	0.37
	F	$k_L = 0.11$ L/mg $Q_m = 2.32\ mg/g$	0.48	0.98	3.63	0.32
Freundlich Isotherm Model (FI)	As	$K_F = 0.18\ n = 1.46$	0.36	0.94	6.93	0.49
	F	$K_F = 0.44\ n = 2.59$	0.19	0.96	4.57	0.41
Three-parameter Toth Isotherm Model (T model)	As	$K_T = 1.16\ a_T = 16.41$ t = 1.31	0.08	0.97	5.41	0.38
	F	$K_T = 0.92\ a_T = 2.16$ t = 1.25	0.09	0.99	2.29	0.20
Modified Langmuir Freundlich Isotherm Model (MLF)	As	$k_L = 0.1008$ $Q_m = 2.72\ mg/g\ n = 1.81$	0.50	0.99	3.80	0.27
	F	$k_L = 0.077$ $Q_m = 2.11\ mg/g\ n = 0.71$	0.57	0.99	1.28	0.19
Redlich Peterson Isotherm Model (RPI)	As	$k_{RP} = 0.11$ $\alpha_{RP} = 0.004$ $\beta = 1.52$	0.48	0.97	5.26	0.37
	F	$k_{RP} = 0.54$ $\alpha_{RP} = 0.51$ $\beta = 0.82$	0.16	0.99	2.10	0.19

Langmuir constant of As(V) was 0.036, and for F, it was 0.11, suggesting the affinity of adsorbate towards adsorbent. The adsorption capacity of AC towards As(V) was 1.54 times greater than that of F, indicating AC was more selective for As(V) than for F. Similar results were obtained in the other research work by Bibi et al. (2015), and Rathore and Mondal (2017). Practically, it was found that the characteristics and the experimental setup can impact the system's selectivity sequence of AC. Due to its reliability and versatility, the Langmuir isotherm model is widely used in sorption studies. It is beneficial for homogeneous sorption processes and is based on the theoretical concept of monolayer adsorption. This model assumes that the interaction forces between adsorbed molecules are insignificant and that a fixed number of energetically equivalent sites are available on the adsorbent surface. Once an adsorbate molecule occupies a site, no further adsorption occurs. Overall, the Langmuir isotherm model provides a straightforward approach to understanding adsorption phenomena [36]. The evaluation of the As(V) separation factor was 0.74, and F was 0.48, which put forward favorable adsorption.

The value of n in the Freundlich model provides insights into the active sites' surface heterogeneity and energy distribution. Usually, the adsorption is favorable when the value of 1/n is more than zero. As(V) showed 0.68, F showed 0.39, which depicts favorable adsorption on AC. If the value of 1/n exceeds unity, it is an unfavorable and irreversible adsorption process. Unlike the Langmuir isotherm, the Freundlich isotherm assumes surface adsorption as a multilayer, and the energy distribution is not uniform on the heterogeneous surface. It also considers the interaction between the adsorbate and the adsorbent. This isotherm may not be applied to the wide range of adsorption data.

Redlich-Peterson isotherm acts as a combination of Langmuir and Freundlich isotherms. The value of β, the exponent values are 1.52 and 0.82 for As(V) and F, respectively. If the value of β is closer to 1, the Langmuir isotherm is preferred. If the value of β is zero, the preferred isotherm is Freundlich. It's a versatile isotherm that can be applied for homogenous or heterogenous adsorption systems. Also, 1/n of the Freundlich model equals (1- β), and when β = 0, it reduces to the Langmuir isotherm. From the Toth isotherm model, the t value of As(V) was 1.31, and F was 1.25. If parameter t's value exceeds unity, it's a heterogenous surface [92].

Considering higher R^2 and lowest RMSE values, the modified Langmuir Freundlich isotherm fits the system more accurately than the other models. Furthermore, the parameter n is the index of heterogeneity in the MLF model (Eq. (10)). When applying a

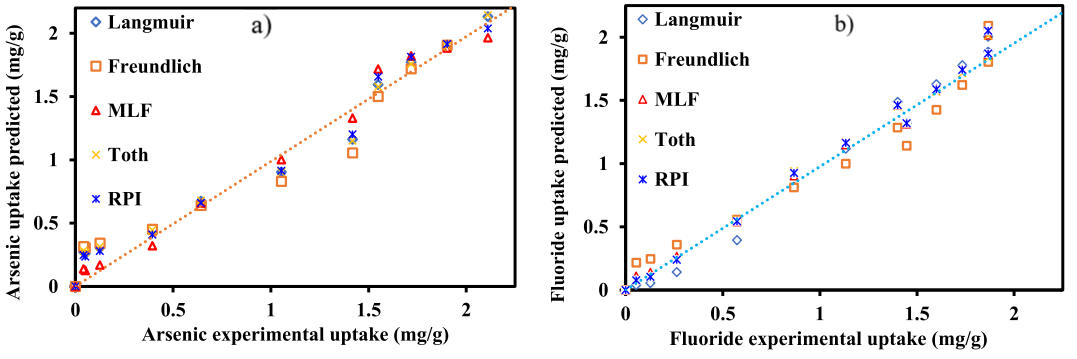

Fig. 11. Comparison between predicted uptake with the best model and experimental uptake of a) arsenic and b) fluoride in a single component system.

heterogeneity index of n, the density function for heterogeneous systems might change in the MLF isotherm, which usually falls between 0 and 1. A homogeneous material has an n value of 1, whereas a heterogeneous material has an n value below 1. In this study, the values of n were 1.81 and 0.71 for As(V) and F, respectively. In the above equation, the affinity constant (K_a) value can be varied for pH-dependent sorption effects. The uniqueness of this isotherm was its pH dependency on adsorption systems. The essential experimental condition required to apply this isotherm model in a system was pH [38]. In conclusion, analysis shows that the modified Langmuir Freundlich model outperformed the other isotherm models by providing the best fit. Its higher R^2 value and lower RMSE error supported this finding, indicating a stronger correlation between the predicted and experimental data points of As(V) and F.

Upon examining Fig. 11(a and b), the relationship between the predicted uptake of arsenic and fluoride, q_{pred}, and the experimental uptake, q_{exp}, was thoroughly investigated to assess the adequacy of the model. The plotted data revealed several straight lines corresponding to the linear graphs associated with the utilized isotherm models. Among the isotherm models considered, namely Langmuir, Freundlich, modified Langmuir Freundlich, Toth, and Redlich Peterson, the modified Langmuir Freundlich model displayed the most favorable fit, which signifies a minor deviation between the predicted and actual experimental measurements [93–95]. Based on the experimental data, the modified Langmuir Freundlich model demonstrated a remarkable ability to predict arsenic and fluoride uptake accurately. Additionally, the comparison of the maximum uptake of As(V) and F with different adsorbents is given in Table 5, which has outcomes similar to those of this present work.

4.6. Competitive adsorption isotherm study

The coexistence of arsenic and fluoride in various areas highlights the significance of studying their simultaneous adsorption. This study aimed to investigate the competitive effects of As(V) and F on AC, focusing on their adsorption behavior in a combined system. The presence of F impacted the behavior of As(V), which was assessed by considering the interaction mechanism and the maximum uptake in binary adsorption systems. By analyzing the interaction mechanisms, it was possible to determine how the presence of F influenced the adsorption behavior of As(V). The study classified the effects of ionic interactions into three categories: synergistic, antagonistic, and no interaction [61,103,104]. These classifications helped to understand the combined adsorption behavior of As(V) and F. The maximum uptake of As(V) and F in the binary system was denoted as Q_{maxB}, while the maximum uptake in the single-component system was denoted as Q_{maxS}, respectively. If the ratio of Q_{maxB} and Q_{maxS} is greater than one, then the mechanism is synergistic. If the ratio is below one, then the effect of the mixture is antagonistic. If the ratio equals one, there is no interaction between the adsorbates in the binary solution [37].

$\frac{Q_{maxB}}{Q_{maxS}} > 1$: The combined effect is more significant than the individual effect in the solution.

$\frac{Q_{maxB}}{Q_{maxS}} = 1$: The solution's combined and individual effects are the same

$\frac{Q_{maxB}}{Q_{maxS}} < 1$: The combined effect is less significant than the individual effect in the solution.

Simultaneous equilibrium experiments were conducted by keeping the fluoride concentration constant at 20 and 30 mg/L while varying the concentration of arsenic from 1 to 100 ppm. The impact of F ions on the adsorption efficiency of As(V) was examined under the same optimized experimental conditions. Similarly, the efficacy of F adsorption was evaluated by altering the concentrations ranging from 1 to 100 ppm while maintaining a constant level of arsenic at 20 and 30 mg/L. Previous literature has such similar studies [41].

Additionally, to evaluate the competitive behavior of the simultaneous systems, the nonlinear extended Langmuir, extended

Table 5
Comparison of maximum adsorption capacity of activated carbon with other adsorbents of binary systems.

No	Adsorbent	Adsorbates dosage		Adsorption capacity		Ref.
		As (mg/L)	F (mg/L)	As (mg/g)	F (mg/g)	
1	Hydrated Cement (10, 20, 30, and 40 g/L)	0.1	5	1.92	1.72	[96]
2	Marble Powder (10, 20, 30, and 40 g/L)	0.1	5	0.04	0.84	[96]
3	Brick Powder (10, 20, 30, and 40 g/L)	0.1	5	0.04	0.18	[96]
4	Thermally treated laterite	1	100	6.43	0.21	[97]
5	Acid-base treated laterite (20 g/L)	0.5	10	0.769	0.526	[61]
6	Aluminum oxide/hydroxide nanoparticles (AHNP)	0.512	6.3	0.833	2	[69]
7	Modified yak dung biochar (10 g/L)	1000	1000	2.926	3.928	[98]
8	Impregnated Ferric hydroxide and Activated Alumina	10	100	0.10	2.42	[99]
9	Chitosan network and a chitosan binary network grafted with N-vinyl caprolactam/N–N-dimethyl acrylamide hydrogels	100–250 μg/L	100–250 μg/L	0.0022	0.150	[100]
10	Bone char	0.25	10	0.7	4.58 ± 0.24	[101]
11	Goethite-coated sand (G-IOCS)	0.25	10	0.5	4.42 ± 0.56	[101]
12	Activated Alumina	0.25	10	0.024	3.16 ± 0.34	[101]
13	Cellulose fibres (1 g/L)	0.05–8.9	11–17	1	2.2	[102]
14	Activated carbon	10	10	2.35	2.28	Present study

Table 6
Competitive isotherm models with inferences.

No	Competitive adsorption Isotherm	Parameters	Features/characteristics	Limitations/Weakness	Ref.
1	**Extended Langmuir/non-modified competitive Langmuir isotherm** $Q_{e,i} = Q_{m,i}\frac{K_{L,i}c_{e,i}}{1+\sum_{j=1}^{N}K_{L,j}c_{e,j}}$	$Q_{m,i}$, $K_{L,i}$	This model is an extension of Langmuir isotherm. The active sites on the adsorbent are assumed to be uniform. The adsorbates have non-interacting adsorption. The equation has the same variables as the modified competitive Langmuir isotherm model except for the interaction factor with only two fitting parameters.	The limitation of this model is isotherm parameters can be completely different in their values for specific adsorbents. Furthermore, the model does not consider interacting adsorption. Though it is a multicomponent isotherm, it does not have competitive parameters. $Q_{m,i}$ is a fitting parameter disconnected from $Qmax,i$ of single component isotherms.	[105]
2	**Extended Langmuir-Freundlich isotherm** $Q_{e,i} = Q_{m,i}\frac{K_{LF,i}c_{e,i}^{\left(1/n_i\right)}}{\sum_{j=1}^{N}K_{LF,i}c_{e,i}^{\left(1/n_i\right)}}$	$Q_{m,i}$, $K_{LF,i}$, n_i	This model is a combination of the Freundlich and Langmuir isotherm models. With the combined isotherms, better results could be achieved. The Langmuir–Freundlich Model is obtained with three fitting parameters based on multicomponent equilibrium data. The parameter K_{LF} describes the intensity of adsorbent–adsorbate interactions, and the parameter "n" represents the heterogeneity and favorability.	The model does not consider interacting adsorption. Though it is a multicomponent isotherm, it does not have interaction parameters. $Q_{m,i}$ is a fitting parameter different from $Q_{max,i}$ of single component isotherms.	[33]
3	**Modified Competitive Langmuir isotherm** $Q_{e,i} = Q_{m,i}\frac{K_{L,i}\left(c_{e,i}/\eta_{L,i}\right)}{1+\sum_{j=1}^{N}K_{L,j}\left(c_{i,j}/\eta_{L,j}\right)}$	$Q_{m,i}$, $K_{L,i}$, $\eta_{L,i}$	This model is an extension of Langmuir isotherm with an interaction term. This model has three fitting parameters. The specific equilibrium condition, maximum adsorption (Q_{max}), the concentration of molecules (C), and the interaction factor (η) depict the competitive effect of adsorbates in the solution, and K describes the Langmuir constant for components.	The model assumed that solute concentration may affect the adsorption and desorption rate. Furthermore, the level of surface heterogeneity may not be considered.	[106]
4	**Jeppu Amrutha Manipal Multicomponent (JAMM) isotherm** $Q_{e,i} = Q_{m,i}\frac{\Phi_i\, x_i\, \left(K_{L,i}\, C_{e,i}\, a_i\right)^{n_i}}{1+\sum_{j=1}^{N}\left(K_{L,i}\, C_{e,i}\, a_i\right)^{n_i}}$	$Q_{m,i}$, Φ_i, x_i, $K_{L,i}$, a_i, n_i	This isotherm is a newly developed multicomponent model from the Langmuir-Freundlich model and includes mole fractions, interaction coefficients, heterogeneity, and affinity parameters. The interaction coefficients predict the competitive behavior of the adsorption system. The JAMM isotherm utilizes the single component parameters to predict the other parameters. There are more parameters and essential factors that previous isotherms ignore and are considered. For example, mole fraction x_i, and the interaction term Φ_i gives more robust predictions.	More data is needed to determine the parameters. Also, there are more parameters.	[42]

Langmuir Freundlich, modified competitive Langmuir, and Jeppu Amrutha Manipal multicomponent, i.e., four multicomponent isotherm models in Table 6, were modeled and simulated, and competitive mechanisms were interpreted. Normalized average percentage error (NAPE), Root mean square errors (RMSE), and correlation coefficients (R^2) were evaluated to validate the model fitting and predicted parameters [33,42].

4.6.1. Competitive adsorption of arsenic with constant fluoride

The binary adsorption system involving various arsenic concentrations and constant fluoride is presented in Fig. 12(a–d). The initial concentration of arsenic ranged from 1 to 100 mg/L, and fluoride concentrations were set at 20 and 30 mg/L. During the competitive isotherm experiments, it was observed that adding fluoride at a constant level of approximately 10 ppm led to a significant reduction in the adsorption of arsenic as As(V). However, when the fluoride concentration was raised to 20, 30, and higher ppm levels, the ability of arsenic to bind to surfaces was slightly affected. The coexistence of fluoride-exhibited mechanisms, including synergism, antagonism, and non-interaction, was also represented in Table 7. Specifically, this study showed arsenic antagonistic behavior in the presence of fluoride [11,107,108].

In summary, the investigation focused on a binary adsorption system involving varying concentrations of arsenic and a constant concentration of fluoride. The addition of fluoride had a notable impact on the adsorption behavior of arsenic, with different mechanisms observed based on their coexistence. Table 7 also provides the model parameters, statistical metrics, and the effect of fluoride-arsenic interaction.

The binary isotherm parameters and error values are displayed in Table 7 for the adsorption of As(V) at constant fluoride. Comparatively, the maximum adsorption capacity of As(V) has been reduced as the intake concentration of fluoride exceeded that of all the above competitive models. The ratio of binary and single maximum uptake of As(V) in all the models suggests antagonistic behavior of As(V) with the addition of F. Increased concentration of fluoride decreased the adsorption of arsenic less significantly, as

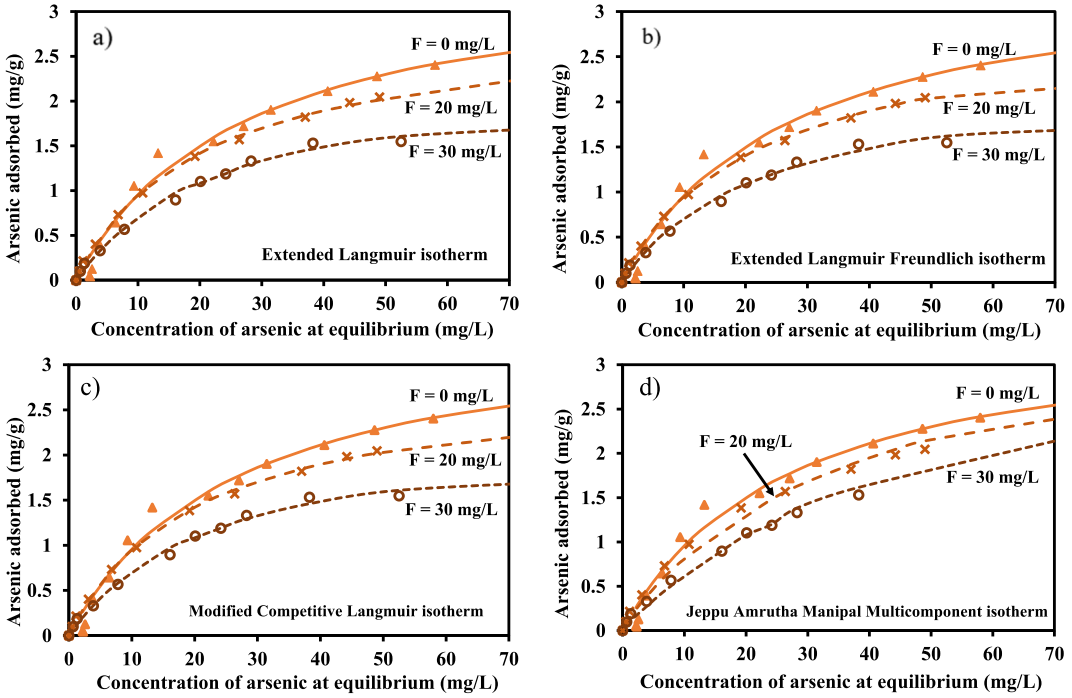

Fig. 12. Competitive isotherm model fit of varying As(V) and constant F.

Table 7
Competitive equilibrium adsorption isotherm parameters and ionic interactions at constant fluoride.

Isotherm Model	Concentrations (mg/L)		Parameters	R^2	NAPE (%)	RMSE	Ratio = Q_{maxB}/Q_{maxS}	Interaction mechanism
	As(V)	F						
Langmuir Isotherm Model	5 to 100	0	$k_L = 0.036$ $Q_m = 3.54\ mg/g$	0.97	3.92	0.05	–	–
Extended Langmuir Isotherm Model (EL)	5 to 100	20	$k_{L,j} = 0.058$ $Q_{m,j} = 2.82\ mg/g$	0.99	1.36	0.08	0.80	Antagonism
		30	$k_{L,j} = 0.312$ $Q_{m,j} = 2.29\ mg/g$	0.99	2.4	0.11	0.65	Antagonism
Extended Langmuir Freundlich Isotherm Model (ELF)	5 to 100	20	$k_{L,j} = 0.056$ $n_j = 0.84$ $Q_{m,j} = 3.12\ mg/g$	0.99	0.88	0.05	0.88	Antagonism
		30	$k_{L,j} = 0.048$ $n_j = 0.88$ $Q_{m,j} = 2.37\ mg/g$	0.99	2.63	0.12	0.67	Antagonism
Modified Competitive Langmuir Isotherm Model (MCL)	5 to 100	20	$k_{L,j} = 0.008$ $\eta_j = 0.17$ $Q_{m,j} = 2.86\ mg/g$	0.99	1.34	0.08	0.81	Antagonism
		30	$k_{L,j} = 0.025$ $\eta_j = 0.25$ $Q_{m,j} = 2.30\ mg/g$	0.99	2.45	0.11	0.65	Antagonism
Jeppu Amrutha Manipal Multicomponent Isotherm Model (JAMM)	5 to 100	20	$k_{L,j} = 0.037$ L/mg $Q_{m,j} = 3.55\ mg/g\ n_j = 0.02$ $\Phi_j = 3.61\ a_j = 2.88$	0.98	3.84	0.23	3.61	Antagonism
		30	$k_{L,j} = 0.036$ L/mg $Q_{m,j} = 3.55\ mg/g\ n_j = 0.01$ $\Phi_j = 3.31\ a_j = 5.28$	0.98	3.01	0.12	3.31	Antagonism

shown in Fig. 12(a – d).

Upon considering the error values, the extended Langmuir Freundlich isotherm has the lowest errors, with an average NAPE of 3.51 and RMSE of 0.17, compared to other models. Additionally, the ELF isotherm, a hybrid model combined with Langmuir and Freundlich

isotherms, prefers to be the EL model if the value of heterogeneity (n) reduces to unity. In extended Langmuir isotherm, the fitting parameters are less, and the errors were 3.76 (NAPE) and 0.19 (RMSE), and the R^2 was 0.99. Even though the EL is the extension of the Langmuir model, it assumes the adsorption surface as homogenous and monolayer adsorption. However, it neglects the interaction between the adsorbates and adsorbents and assumes that the energy of active sites is uniform. The average errors of MCL isotherm were 3.79 (NAPE) and 0.19 (RMSE), which showed a better fit with R^2 values of 0.99. Though the interaction factor η gives the interaction between the adsorbate and adsorbent in the MCL model if the value of η reduces to unity, the MCL isotherm behaves as the EL isotherm model, and the fitting parameters are more.

JAMM isotherm is a newly developed model from our previous work [42] that includes mole fractions, interaction coefficients, heterogeneity, and affinity parameters. There are more fitting parameters, but the model considers many ignored factors in multi-component adsorption isotherms. JAMM isotherm leverages the single component parameters to forecast the additional parameters. Within this model, the heterogeneity index plays a vital role in discerning between the homogenous or heterogenous surfaces; heterogeneity is indicated as the n value was below one. Moreover, the interaction coefficient elucidates the impact of one pollutant's presence on the adsorption of another. The affinity factor provides insight into the adsorbate preferences for accessing the surface of the AC. Furthermore, the mole fractions encompass each molecule and its driving forces within a competitive adsorption system. The NAPE was 6.85, and the RMSE was 0.35, with 0.98 as the R^2 value of the JAMM model. This isotherm model also fits the As(V) and F simultaneous system well. Therefore, the order of the goodness of fitting isotherm was extended Langmuir Freundlich > extended Langmuir > modified competitive Langmuir > Jeppu Amrutha Manipal Multicomponent, in varying arsenic at a fluoride constant.

4.6.2. Competitive adsorption of fluoride with constant arsenic

The binary adsorption system with various fluoride concentrations and constant arsenic is illustrated in Fig. 13(a -b). The initial concentration of fluoride ranged from 1 to 100 mg/L. In contrast, the concentrations of arsenic were set at 20 and 30 mg/L. The competitive isotherm experiments revealed a notable decrease in fluoride adsorption upon adding approximately 10 ppm of arsenic. However, as the concentration of arsenic was raised to 20, 30, and higher ppm levels, the ability of fluoride to bind to surfaces was less affected. In this study, Table 8 presents the parameters, coefficient of determination (R^2), root mean square error (RMSE), and normalized average percentage error (NAPE) for each model used in the analysis. The coexistence of arsenic demonstrated antagonistic behavior, as shown in Table 8.

In summary, the study investigated the competitive adsorption of fluoride and arsenic in a binary system. The concentration of arsenic affected the adsorption behavior of fluoride, with a significant impact observed at around 10 ppm of arsenic. However, higher concentrations of arsenic had a comparatively greater effect on fluoride uptake.

The binary isotherm parameters and error values are shown in Table 8 for the adsorption of F at constant arsenic. The maximum adsorption capacity of F was reduced as the intake concentration of the arsenic increased. The ratio of binary and single maximum uptake of F in all the models suggests that F showed antagonistic behavior with the addition of As(V). There was a slight decrease in the

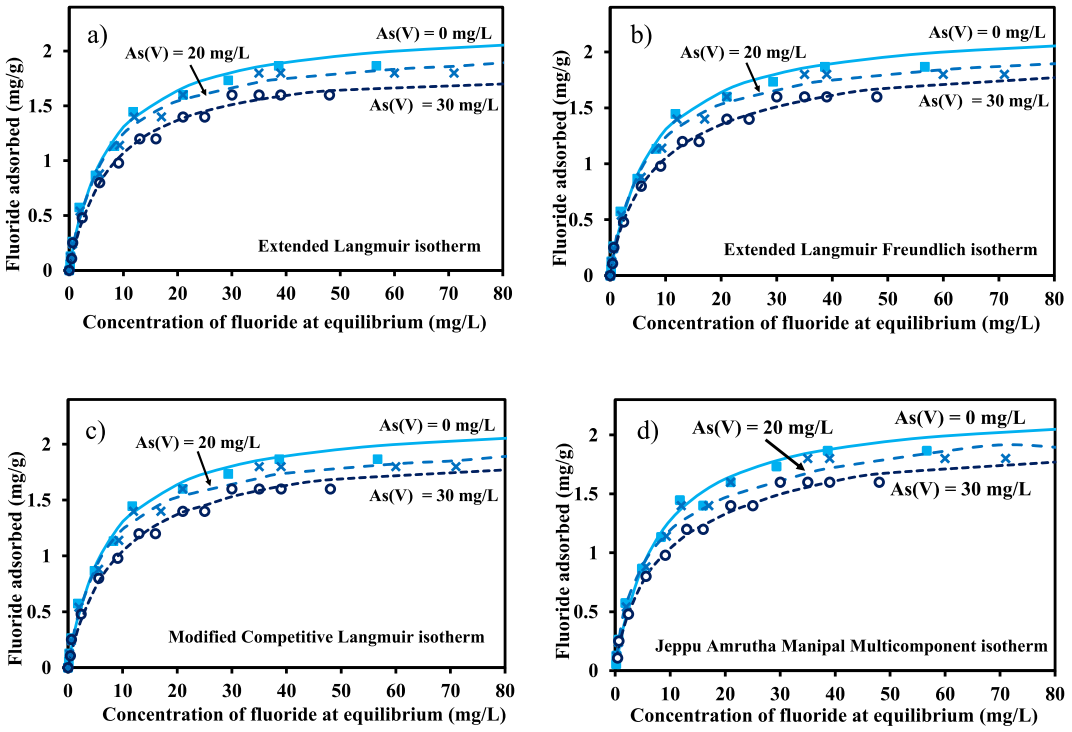

Fig. 13. Competitive isotherm model fit of varying F and constant As(V).

Table 8
Competitive equilibrium adsorption isotherm parameters and ionic interactions at constant arsenic.

Isotherm Model	Concentrations (mg/L)		Parameters	R^2	NAPE (%)	RMSE	Ratio = Q_{maxB}/Q_{maxS}	Interaction mechanism
	F	As (V)						
Langmuir Isotherm Model	5 to 100	0	$k_L = 0.14$ $Q_m = 2.24\ mg/g$	0.98	0.53	0.25	–	–
Extended Langmuir Isotherm Model (EL)	5 to 100	20	$k_L = 0.16$ $Q_m = 2.03\ mg/g$	0.98	3.32	0.20	0.90	Antagonism
		30	$k_L = 0.13$ $Q_m = 1.91\ mg/g$	0.98	2.58	0.15	0.85	Antagonism
Extended Langmuir Freundlich Isotherm Model (ELF)	5 to 100	20	$k_{L,i} = 0.17$ $n_i = 1.08$ $Q_{m,j} = 2.08\ mg/g$	0.98	3.15	0.19	0.93	Antagonism
		30	$k_{L,i} = 0.18$ $n_i = 1.20$ $Q_{m,i} = 2.14\ mg/g$	0.99	2.33	0.13	0.95	Antagonism
Modified Competitive Langmuir Isotherm Model (MCL)	5 to 100	20	$k_{L,i} = 0.30$ $\eta_i = 0.45$ $Q_{m,i} = 2.04\ mg/g$	0.98	3.41	0.21	0.91	Antagonism
		30	$k_{L,i} = 0.47$ $\eta_i = 0.16$ $Q_{m,i} = 2\ mg/g$	0.98	2.83	0.16	0.89	Antagonism
Jeppu Amrutha Manipal Multicomponent Isotherm Model (JAMM) [42]	5 to 100	20	$k_{L,i} = 0.036$ L/mg $Q_{m,i} = 2.24\ mg/g\ n_i = 0.30$ $\Phi_i = 1.42\ a_i = 7.61$	0.99	3.46	0.21	1.42	Antagonism
		30	$k_{L,i} = 0.036$ L/mg $Q_{m,i} = 2.24\ mg/g\ n_i = 0.27$ $\Phi_i = 1.42\ a_i = 8.39$	0.99	2.13	0.12	1.42	Antagonism

fluoride adsorption when the As(V) concentration increased, as shown in Fig. 13(a–d), which indicated that the fluoride adsorption was more affected by the presence of As(V).

Consequently, the extended Langmuir Freundlich isotherm's error values have the lowest errors, with an average NAPE of 5.48 and RMSE of 0.32, compared to other models. The Jeppu Amrutha Manipal Multicomponent isotherm includes mole fractions, interaction coefficients, heterogeneity index, and affinity parameters. Amongst simulated isotherm models, the ignored fitting parameters are considered in the JAMM model. JAMM isotherm was modeled by considering the single component parameters to simulate binary component parameters. The heterogeneity index 'n' value was below one in all the variations, predicting a heterogeneous surface. Moreover, As(V) and F's interaction coefficients were also determined. The higher the interaction coefficient, the more significant the adsorption. As predicted, As(V) showed better adsorption interaction than F. The JAMM isotherm predicted the fitting parameters with NAPE was 5.59, and the RMSE was 0.33, with 0.99 as the R^2 values. In the extended Langmuir isotherm, the errors were 5.9 (NAPE) and 0.35 (RMSE), and the R^2 was 0.99. The average errors of MCL isotherm were 6.24 (NAPE) and 0.37 (RMSE), which showed a better fit with R^2 values of 0.99. In conclusion, all the models accurately predicted and simulated the parameters with low errors and greater R^2 values. The multicomponent isotherm models accurately fit the As(V) and F simultaneous systems. Therefore, the order of the goodness of fitting isotherm was extended Langmuir Freundlich > Jeppu Amrutha Manipal Multicomponent > extended Langmuir > modified competitive Langmuir, in varying fluoride at an arsenic constant.

The results indicate that when competitive ions of fluoride increase, the removal capacity of arsenic decreases, and vice versa. It was observed that the adsorption performances were slightly lower in binary systems compared to single systems. This can be attributed to the competition between ions to access the active sites on the adsorbent and the affinity of the ions towards the AC. The specific properties and behavior of the ions in the binary system are also considered, including electronegativity, hydrated radii, ion diffusivity, suitable site properties for uptake, formation of hydroxyl complexes, surface charge density, and surface attractivity ratio (as shown in Table 9) [33,79,111].

One significant factor influencing competitive adsorption is hydrated radii. As(V) hydrated radii are 2–2.2 Å, while for F is 3.52 Å. Higher hydrated radii indicate lower accessibility to the surface and pores of AC. Consequently, As(V) adsorbs more rapidly than fluoride in simultaneous adsorption. The affinity and suitability of As(V) and F for AC also contribute to the competition between the ions in the solution. However, the maximum uptake of arsenic was higher than that of fluoride. From our previous study by Acharya et al. (2023), the measured surface attractivity ratio for As(V) was 1.4, exceeding F, suggesting the preference adsorption of As(V) over F, as in Table 8. As the surface charge density influences the electrostatic interactions, the surface charge density of the As(V) was greater than the F, indicating more interactions of As(V) with AC than F [42]. The equilibrium adsorption capacity follows As(V) > F in simultaneous adsorption. When the fluoride concentration increases in an arsenic solution, fluoride has a slight impact on the uptake of arsenic. Similarly, when the arsenic concentration increases in a fluoride solution, arsenic alters the fluoride uptake.

Table 9
Molecular and ionic properties of As(V) and F.

No	Properties	As(V)	F	References
1	Species	$HAsO_4^{2-}$, H_3AsO_4, $H_2AsO_4^-$	F^-	[42,109,110]
2	Hydrated radii (Å)	>2–2.2	3.52	
3	Ionic radii (Å)	0.39	1.19	
4	Electronegativity (Pauling)	2.18	3.98	
5	Ion diffusivity (10^{-9} m^2/S)	0.323	1.46	
6	Surface area (SA) ($Å^2$)	60.82	155.70	
7	Surface charge density (Pauling/$Å^2$)	0.0358	0.0256	
8	Percentage surface charge density (Pauling/$Å^2$)	3.58	2.56	
9	surface attractivity ratio	1.4	0.71	

4.7. Desorption and regeneration of activated carbon

The regeneration of the AC was investigated. The adsorption experiments with the initial concentration of 100 mg/L of As(V) and F, dosage of 5 g/L, volume of 50 mL, pH of 5, and agitation speed of 150 rpm were performed. The uptake of As(V) and F was measured. The regeneration studies were carried out for the adsorbed AC utilized in single and binary adsorption of As(V) and F. After the adsorption, the AC was treated with various eluting reagents like 0.1 M NaOH, 0.1 M HCl, and distilled water for desorption studies [43].

The desorption percentage of AC was gauged after each consecutive desorption cycle by Eq (18). The performances of the reused AC were investigated for three cycles for F and five cycles for As(V), as shown in Fig. 14(a–d). The desorption efficiency decreased slightly with successive As(V) and F cycles. In the case of desorption of a single system of As(V), the efficiency reduced from 21.55 % to 17.39 % by using NaOH, 20.2 %–14.94 % with HCl, and from 20.08 % to 15.13 % by water. Consequently, for F in a single desorption system, the efficiency reduced from 11.35 % to 9.98 % by using NaOH, 14.08 %–13.03 % with HCl, and from 29.54 % to 28.67 % by water. F's efficiency in binary systems was somewhat reduced when employing NaOH (31.85 %–30.6 %), HCl (21.35 %–20.53 %), and water (28.15 %–27.71 %). Comparably, As(V) desorption in binary systems dropped while utilizing NaOH (14.78 %–10.55 %), HCl (8.45 %–4.68 %), and water (24.42 %–21.5 %). Notably, NaOH showed out as an efficient eluent for removing As(V) and F. It was also observed that the desorption in the binary system was greater than that in the single-component system. The desorption system's decreased efficiency is given in supplementary data Table S9 in supplementary data.

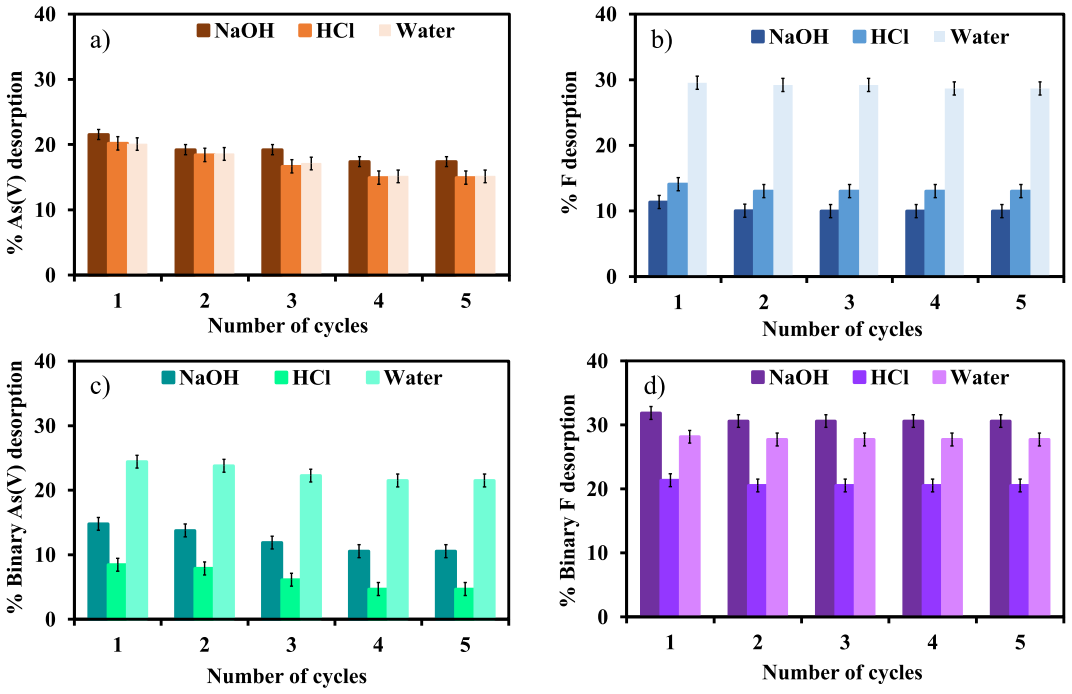

Fig. 14. Desorption efficiency of a) As(V), b) F and c) As(V) in binary system d) F in binary system.

5. Discussion

This study leverages a multi-faceted analytical approach, including BET, FTIR, XRD, FESEM, and EDS, unraveling the intricate characterization of AC and its adsorption behavior as an adsorbent for arsenic and fluoride simultaneously. The EDS and XRD confirmed the essential components of AC composition. The influence of dosage, pH, and contact time were examined in single and simultaneous adsorption systems. The optimum conditions for better performance were 5 g/L of dosage, pH 5, and a contact time of 48 h. In single-component systems, AC demonstrates efficient adsorption of arsenic and fluoride, achieving a percentage removal of 93.56 % for arsenic and 72 % for fluoride.

Meanwhile, for proficiency in dealing with binary-component systems, the percentage removal of As(V) was 71.91 %, while fluoride was removed at a rate of 90 %. The coexistence and competition of arsenic and fluoride complicate the removal in competitive systems. The results analyzed AC's adsorption potential, surface area, pore volume, and size, indicating that it falls within the mesoporous range. The AC exhibits a point of zero charges (pH_{zpc}) at approximately pH 6.8. to analyze a material's surface charge. Additionally, experimental data for arsenic and fluoride adsorption using AC indicates that maximum adsorption occurs at pH 3; strong acidic pH was well preferred. The adsorption rate of As(V) and F prefers lower pH, possibly due to the negatively charged surface of the adsorbent at higher pH levels. Consequently, As(V) and fluoride significantly adsorb better at lower solution pH in simultaneous removal, implying that the surface of AC was positively charged as the pH of the solution was less than pH_{zpc}.

In the kinetic studies, the pseudo-second-order equation best describes the adsorption process, evident by a coefficient of determination (R^2) approaching 1 and linearity observed in the t/q_t vs. t plot. The reaction rate constants for As(V) and F in single-component systems suggested fluoride adsorption was quicker than arsenic. In competitive adsorption, the kinetics of As(V) showed antagonistic behavior with reduced experimental values. Conversely, F displayed synergistic behavior, particularly with As(V) presence in low initial concentrations. The synergy implies As(V) might enhance the adsorption of F, a phenomenon that adds complexity to the competitive dynamics. To elaborate further, sorption isotherms were simulated to determine model parameters. The findings illustrated that AC's adsorption capacity was proved to be substantially more pronounced for As(V) than fluoride in a single-component system with identical experimental conditions. In the single-component system, the maximum uptake for fluoride was 2.32 mg/g, while arsenic was 3.58 mg/g according to the Langmuir model at pH 5. The substantial difference between the two species shows the superior affinity of AC for As(V). The sorption uptake of AC towards As(V) was remarkably 1.54 times greater than that of F. This disparity in selectivity underscores the AC chooses As(V) over F. Also, the modified Langmuir Freundlich isotherm model with higher R^2 and lowest RMSE showed the best fit for As(V) and F.

Moreover, the competitive studies divulge crucial insights into selectivity adsorption, and the presence of fluoride displayed antagonistic behavior as it coexists with arsenic. The antagonism describes a discernible reduction in the maximum uptake of arsenic within the binary adsorption system. Specifically, with the coexistence of fluoride, the maximum uptake of arsenic diminishes to 2.35 mg/g. An even higher F concentration of 20 mg/L further decreases to 2.20 mg/g, and with 30 mg/L fluoride, As(V) uptake has no significant change. Thus, these findings illustrated that the interference of F profoundly affected the uptake of As(V).

Interestingly, the concentration of arsenic was found to impact the behavior of fluoride adsorption, with a significant influence observed at around 20 mg/L of arsenic. Also, higher concentrations of arsenic had a comparatively more significant effect on fluoride uptake. The comparative analysis of various adsorption isotherm models reveals significant distinctions in the intricacies of adsorption processes. Among these models, the extended Langmuir isotherm lacks the capacity to elucidate any competitive parameters. Conversely, the extended Langmuir Freundlich isotherm offers insights into the heterogeneity of the adsorbed surface. The modified competitive Langmuir isotherm model in binary adsorption studies highlights the interaction between As(V) and F. However, the Jeppu Amrutha Manipal Multicomponent isotherm encompasses the mole fractions, interaction coefficients, heterogeneity index, and affinity factor, which were neglected in most multicomponent isotherm models. It was evident that when competitive fluoride ions increase, the removal of arsenic proportionally diminishes, and vice versa. This phenomenon can be attributed to the intensified competition between ions vying to access the active sites on the adsorbent, as well as the affinity of the ions towards the AC. The competition might contribute to the nuanced differences in adsorption efficiencies.

Additionally, AC regeneration was conducted to confirm its effectiveness and reusability. Five cycles of analyzing the effects of repurposed AC decreased the desorption efficiency of As(V) and F. When desorption of a single As(V) system, the efficiency reduced from 21.55 % to 17.39 % using NaOH, 20.2 %–14.94 % with HCl, and from 20.08 % to 15.13 % by water. Consequently, F in a single desorption system reduced efficiency from 11.35 % to 9.98 % using NaOH, 14.08 %–13.03 % with HCl, and from 29.54 % to 28.67 % by water. In binary systems, a minor reduction in the efficiency of F from 31.85 % to 30.6 % using NaOH, 21.35 %–20.53 % using HCl, and 28.15 %–27.71 % by water. Similarly, As(V) desorption in binary systems dropped from 14.78 % to 10.55 % using NaOH, 8.45 %–4.68 % with HCl, and 24.42 %–21.5 % by water, amongst, NaOH proved to be efficient eluent. One notable observation was that the adsorption performances might be slightly lower in binary systems compared to their counterparts in single systems.

6. Conclusion

To conclude, activated carbon was used to adsorb arsenic and fluoride to study the co-removal of arsenic and fluoride. Several crucial parameters like pH, temperature, initial concentration, agitation speed, adsorbent dosage, and equilibrium time were found to govern arsenic and fluoride adsorption in single and binary systems. Applying kinetic and equilibrium isotherm models helps unravel the nature of adsorption and its complex interaction phenomena. Single-component isotherm models were simulated using the Langmuir, Freundlich, modified Langmuir isotherm, Toth, and Redlich-Peterson's models. The modeling and simulations of competitive adsorption were done using extended Langmuir, extended Langmuir Freundlich, modified competitive Langmuir, and

Jeppu Amrutha Manipal Multicomponent isotherms for multi-component systems. These models gave insights into adsorption, such as maximum adsorption capacity, affinity, and the competitive interaction. These models played a crucial role in understanding the adsorption process and the behavior exhibited by arsenic and fluoride in competitive systems. These models also help determine the synergetic, antagonistic, and no-interaction behavior.

Additionally, the study explored the interaction mechanisms, kinetics, competitive isotherm modeling, and adsorption properties by analyzing the adsorbent's and adsorbate's equilibrium data. By comprehensively examining the adsorption behavior of arsenic and fluoride on AC, this study contributes to a deeper understanding of their removal mechanisms. The findings from this research have the potential to advise the development of efficient adsorption processes and provide valuable insights for water treatment applications. The modeling studies unveiled a nuanced hierarchy of isotherm fitting, with extended Langmuir Freundlich > extended Langmuir > modified competitive Langmuir > Jeppu Amrutha Manipal Multicomponent model in varying arsenic at a constant fluoride and extended Langmuir Freundlich > Jeppu Amrutha Manipal Multicomponent > extended Langmuir > modified competitive Langmuir model in varying fluoride at constant arsenic. All the model parameters are estimated by nonlinear regression analysis, minimizing errors, and ensuring the attainment of better R^2 values. The interaction of AC with arsenic and fluoride was assessed in competitive adsorption. Upon analyzing the results, we found that arsenic and fluoride behaved antagonistically in the presence of each other, and AC showed more selectivity towards As(V) than F. The regeneration studies showed the reusability of AC for single and simultaneous removal. These insights provide a comprehensive understanding of the simultaneous removal of arsenic and fluoride.

Ethical approval

The authors declare that ethical considerations were considered while writing the manuscript.

Consent to participate

The experimental paper does not involve human subjects.

Consent to publish

We declare that there is no conflict of interest associated with this manuscript. As the corresponding author, we confirm that the manuscript has been proofread and approved for submission by all named authors.

Funding

The current work has not received any form of funding from the agencies.

Data availability statement

The data generated and analyzed during this work will be presented on request.

CRediT authorship contribution statement

Amrutha Acharya: Writing – original draft, Validation, Software, Methodology, Investigation, Formal analysis, Data curation, Conceptualization. **Gautham Jeppu:** Writing – review & editing, Validation, Supervision, Project administration. **Chikmagalur Raju Girish:** Writing – review & editing, Validation, Supervision, Project administration. **Balakrishna Prabhu:** Writing – review & editing, Project administration. **Vytla Ramachandra Murty:** Writing – review & editing, Project administration. **Alita Stephy Martis:** Investigation. **Shrividya Ramesh:** Investigation.

Declaration of competing interest

The authors declare that they have no known competing financial interests or personal relationships that could have appeared to influence the work reported in this paper.

Appendix A. Supplementary data

Supplementary data to this article can be found online at https://doi.org/10.1016/j.heliyon.2024.e31967.

References

[1] V.N. Scheverin, A. Russo, M. Grünhut, M.F. Horst, S. Jacobo, V.L. Lassalle, Novel iron-based nanocomposites for arsenic removal in groundwater: insights from their synthesis to implementation for real groundwater remediation, Environ. Earth Sci. 81 (7) (2022) 1–15, https://doi.org/10.1007/s12665-022-10286-z.

[2] P.L. Smedley, Sources and distribution of arsenic in groundwater and aquifers, Arsen. Groundw. a World Probl. (1993) 1–34.
[3] A.M. Ingallinella, V.A. Pacini, R.G. Fernández, R.M. Vidoni, G. Sanguinetti, Simultaneous removal of arsenic and fluoride from groundwater by coagulation-adsorption with polyaluminum chloride, J. Environ. Sci. Heal. - Part A Toxic/Hazardous Subst. Environ. Eng. 46 (11) (2011) 1288–1296, https://doi.org/10.1080/10934529.2011.598835.
[4] N. Abdullah, N. Yusof, W.J. Lau, J. Jaafar, A.F. Ismail, Recent trends of heavy metal removal from water/wastewater by membrane technologies, J. Ind. Eng. Chem. 76 (2019) 17–38, https://doi.org/10.1016/j.jiec.2019.03.029.
[5] K.D. Brahman, et al., Biosorptive removal of inorganic arsenic species and fluoride from aqueous medium by the stem of Tecomella undulate, Chemosphere 150 (2016) 320–328, https://doi.org/10.1016/j.chemosphere.2016.02.017.
[6] N.C. Srivastava, I.W. Eames, A review of adsorbents and adsorbates in solid-vapour adsorption heat pump systems, Appl. Therm. Eng. 18 (9–10) (1998) 707–714, https://doi.org/10.1016/S1359-4311(97)00106-3.
[7] Y. Yu, Z. Zhou, Z. Ding, M. Zuo, J. Cheng, C. Jing, Simultaneous arsenic and fluoride removal using {201}TiO2–ZrO2: Fabrication, characterization, and mechanism, J. Hazard Mater. 377 (May) (2019) 267–273, https://doi.org/10.1016/j.jhazmat.2019.05.060.
[8] Y.H. Xu, T. Nakajima, A. Ohki, Adsorption and removal of arsenic(V) from drinking water by aluminum-loaded Shirasu-zeolite, J. Hazard Mater. 92 (3) (2002) 275–287, https://doi.org/10.1016/S0304-3894(02)00020-1.
[9] S. Bibi, M.A. Kamran, J. Sultana, A. Farooqi, Occurrence and methods to remove arsenic and fluoride contamination in water, Environ. Chem. Lett. 15 (1) (2017) 125–149, https://doi.org/10.1007/s10311-016-0590-2.
[10] S.M. Prabhu, C. Chuaicham, C.M. Park, B.H. Jeon, K. Sasaki, Synthesis and characterization of defective UiO-66 for efficient co-immobilization of arsenate and fluoride from single/binary solutions, Environ. Pollut. 278 (2021) 116841, https://doi.org/10.1016/j.envpol.2021.116841.
[11] S.V. Jadhav, E. Bringas, G.D. Yadav, V.K. Rathod, I. Ortiz, K.V. Marathe, Arsenic and fluoride contaminated groundwaters: a review of current technologies for contaminants removal, J. Environ. Manage. 162 (2015) 306–325, https://doi.org/10.1016/j.jenvman.2015.07.020.
[12] N. Sahu, J. Singh, J.R. Koduru, Removal of arsenic from aqueous solution by novel iron and iron–zirconium modified activated carbon derived from chemical carbonization of Tectona grandis sawdust: isotherm, kinetic, thermodynamic and breakthrough curve modelling, Environ. Res. 200 (March) (2021) 111431, https://doi.org/10.1016/j.envres.2021.111431.
[13] S.T. Ramesh, N. Rameshbabu, R. Gandhimathi, P.V. Nidheesh, M. Srikanth Kumar, Kinetics and equilibrium studies for the removal of heavy metals in both single and binary systems using hydroxyapatite, Appl. Water Sci. 2 (3) (2012) 187–197, https://doi.org/10.1007/s13201-012-0036-3.
[14] M. Mourabet, A. El Rhilassi, H. El Boujaady, M. Bennani-Ziatni, R. El Hamri, A. Taitai, Removal of fluoride from aqueous solution by adsorption on hydroxyapatite (HAp) using response surface methodology, J. Saudi Chem. Soc. 19 (6) (2015) 603–615, https://doi.org/10.1016/j.jscs.2012.03.003.
[15] L. Yuan, et al., Influences of pH and metal ions on the interactions of oxytetracycline onto nano-hydroxyapatite and their co-adsorption behavior in aqueous solution, J. Colloid Interface Sci. 541 (2019) 101–113, https://doi.org/10.1016/j.jcis.2019.01.078.
[16] B. Park, S.M. Ghoreishian, Y. Kim, B.J. Park, S.M. Kang, Y.S. Huh, Dual-functional micro-adsorbents: Application for simultaneous adsorption of cesium and strontium, Chemosphere 263 (2021) 128266, https://doi.org/10.1016/j.chemosphere.2020.128266.
[17] Chiban Mohamed, Application of low-cost adsorbents for arsenic removal: a review, J. Environ. Chem. Ecotoxicol. 4 (5) (2012), https://doi.org/10.5897/jece11.013.
[18] H. Jiang, et al., Defluoridation investigation of Yttrium by laminated Y-Zr-Al tri-metal nanocomposite and analysis of the fluoride sorption mechanism, Sci. Total Environ. 648 (2019) 1342–1353, https://doi.org/10.1016/j.scitotenv.2018.08.258.
[19] A. Haldar, S. Ray, Arsenic and fluoride problems of groundwater in West Bengal and available technologies for remediation, Int. J. Innov. Res. Comput. Commun. Eng. 3 (6) (2014) 135–141.
[20] M.S. Onyango, H. Matsuda, Chapter 1 fluoride removal from water using adsorption technique, Adv. Fluor. Sci. 2 (C) (2006) 1–48, https://doi.org/10.1016/S1872-0358(06)02001-X.
[21] F. Bullough, D.J. Weiss, W.E. Dubbin, J.C. Barry, Julia Barrott, K.S. Arup, Evidence of competitive adsorption of Sb(III) and As(III) on activated alumina, Ind. Eng. Chem. Res. 49 (5) (2010) 2521–2524, https://doi.org/10.1021/ie901061x.
[22] Y. Yin, T. Zhou, H. Luo, J. Geng, W. Yu, Z. Jiang, Adsorption of arsenic by activated charcoal coated zirconium-manganese nanocomposite: performance and mechanism, Colloids Surfaces A Physicochem. Eng. Asp. 575 (April) (2019) 318–328, https://doi.org/10.1016/j.colsurfa.2019.04.093.
[23] T. Pang, T.S. Aye Chan, Y.A.C. Jande, J. Shen, Removal of fluoride from water using activated carbon fibres modified with zirconium by a drop-coating method, Chemosphere 255 (2020) 126950, https://doi.org/10.1016/j.chemosphere.2020.126950.
[24] M. Chaudhary, N. Jain, A. Maiti, A comparative adsorption kinetic modeling of fluoride adsorption by nanoparticles and its polymeric nanocomposite, J. Environ. Chem. Eng. 9 (5) (2021) 105595, https://doi.org/10.1016/j.jece.2021.105595.
[25] S.S. Salih, A. Mahdi, M. Kadhom, T.K. Ghosh, Competitive adsorption of As(III) and As(V) onto chitosan/diatomaceous earth adsorbent, J. Environ. Chem. Eng. 7 (5) (2019) 103407, https://doi.org/10.1016/j.jece.2019.103407.
[26] S.I. Alhassan, et al., A review on fluoride adsorption using modified bauxite: surface modification and sorption mechanisms perspectives, J. Environ. Chem. Eng. 8 (6) (2020) 104532, https://doi.org/10.1016/j.jece.2020.104532.
[27] M. Karnib, A. Kabbani, H. Holail, Z. Olama, Heavy metals removal using activated carbon, silica and silica activated carbon composite, Energy Proc. 50 (2014) 113–120, https://doi.org/10.1016/j.egypro.2014.06.014.
[28] W. Xiang, G. Zhang, Y. Zhang, D. Tang, J. Wang, Synthesis and characterization of cotton-like Ca-Al-La composite as an adsorbent for fluoride removal, Chem. Eng. J. 250 (2014) 423–430, https://doi.org/10.1016/j.cej.2014.03.118.
[29] H. Goyal, P. Mondal, Life cycle assessment (LCA) of the arsenic and fluoride removal from groundwater through adsorption and electrocoagulation: a comparative study, Chemosphere 304 (June) (2022) 135243, https://doi.org/10.1016/j.chemosphere.2022.135243.
[30] T. Radu, A. Kumar, T.P. Clement, G. Jeppu, M.O. Barnett, Development of a scalable model for predicting arsenic transport coupled with oxidation and adsorption reactions, J. Contam. Hydrol. 95 (1–2) (2008) 30–41, https://doi.org/10.1016/j.jconhyd.2007.07.004.
[31] L. Dambies, Existing and prospective sorption technologies for the removal of arsenic in water, Separ. Sci. Technol. 39 (3) (2005) 603–627, https://doi.org/10.1081/ss-120027997.
[32] R. Manju, A.M. Hegde, P. Parlees, A. Keshan, Environmental arsenic contamination and its effect on intelligence quotient of school children in a historic gold mining area Hutti, North Karnataka, India: a pilot study, J. Neurosci. Rural Pract. 8 (3) (2017) 364–367, https://doi.org/10.4103/jnrp.jnrp_501_16.
[33] G. Jeppu Amrutha, C.R. Girish, B. Prabhu, K. Mayer, Multi-component adsorption isotherms : review and modeling studies, Environ. Process. (2023), https://doi.org/10.1007/s40710-023-00631-0.
[34] Y.H. Li, et al., Competitive adsorption of Pb2+, Cu2+ and Cd 2+ ions from aqueous solutions by multiwalled carbon nanotubes, Carbon N. Y. 41 (14) (2003) 2787–2792, https://doi.org/10.1016/S0008-6223(03)00392-0.
[35] E.A. Ofudje, I.A. Adeogun, M.A. Idowu, S.O. Kareem, N.A. Ndukwe, Simultaneous removals of cadmium(II) ions and reactive yellow 4 dye from aqueous solution by bone meal-derived apatite: kinetics, equilibrium and thermodynamic evaluations, J. Anal. Sci. Technol. 11 (1) (2020), https://doi.org/10.1186/s40543-020-0206-0.
[36] M.A. Al-Ghouti, D.A. Da'ana, Guidelines for the use and interpretation of adsorption isotherm models: a review, J. Hazard Mater. 393 (February) (2020) 122383, https://doi.org/10.1016/j.jhazmat.2020.122383.
[37] C.R. Girish, Various isotherm models for multicomponent adsorption: a review, Int. J. Civ. Eng. Technol. 8 (10) (2019) 80–86.
[38] G.P. Jeppu, T.P. Clement, A modified Langmuir-Freundlich isotherm model for simulating pH-dependent adsorption effects, J. Contam. Hydrol. 129 (130) (2012) 46–53, https://doi.org/10.1016/j.jconhyd.2011.12.001.
[39] M.S. Berber-Mendoza, J.I. Martínez-Costa, R. Leyva-Ramos, H.J. Amezquita Garcia, N.A. Medellín Castillo, Competitive adsorption of heavy metals from aqueous solution onto oxidized activated carbon fiber, Water Air Soil Pollut. 229 (8) (2018), https://doi.org/10.1007/s11270-018-3906-y.
[40] J. Zhu, A.M. Katti, G. Guiochon, Comparison of various isotherm models for predicting competitive adsorption data, J. Chromatogr. A 552 (C) (1991) 71–89, https://doi.org/10.1016/S0021-9673(01)95924-2.

[41] A. Terdputtakun, O. anong Arqueropanyo, P. Sooksamiti, S. Janhom, W. Naksata, Adsorption isotherm models and error analysis for single and binary adsorption of Cd(II) and Zn(II) using leonardite as adsorbent, Environ. Earth Sci. 76 (22) (2017) 1–11, https://doi.org/10.1007/s12665-017-7110-y.

[42] A. Acharya, G. Jeppu, C.R. Girish, B. Prabhu, Development of a Multicomponent Adsorption Isotherm Equation and its Validation by Modeling, 2023, https://doi.org/10.1021/acs.langmuir.3c02496.

[43] A.R. Gupta, V.C. Joshi, A. Yadav, S. Sharma, Synchronous removal of arsenic and fluoride from aqueous solution: a facile approach to fabricate novel functional metallopolymer microspheres, ACS Omega 7 (6) (2022) 4879–4891, https://doi.org/10.1021/acsomega.1c05456.

[44] M. Arshadi, M. Soleymanzadeh, J.W.L. Salvacion, F. SalimiVahid, Nanoscale Zero-Valent Iron (NZVI) supported on sineguelas waste for Pb(II) removal from aqueous solution: kinetics, thermodynamic and mechanism, J. Colloid Interface Sci. 426 (2014) 241–251, https://doi.org/10.1016/j.jcis.2014.04.014.

[45] B. Kakavandi, et al., Simultaneous adsorption of lead and aniline onto magnetically recoverable carbon: optimization, modeling and mechanism, J. Chem. Technol. Biotechnol. 91 (12) (2016) 3000–3010, https://doi.org/10.1002/jctb.4925.

[46] M. Oveisi, M.A. Asli, N.M. Mahmoodi, MIL-Ti metal-organic frameworks (MOFs) nanomaterials as superior adsorbents: synthesis and ultrasound-aided dye adsorption from multicomponent wastewater systems, J. Hazard Mater. 347 (2018) 123–140, https://doi.org/10.1016/j.jhazmat.2017.12.057.

[47] Y. Deng, S. Huang, D.A. Laird, X. Wang, Z. Meng, Adsorption behaviour and mechanisms of cadmium and nickel on rice straw biochars in single- and binary-metal systems, Chemosphere 218 (2019) 308–318, https://doi.org/10.1016/j.chemosphere.2018.11.081.

[48] D. Yu, L. Wang, M. Wu, Simultaneous removal of dye and heavy metal by banana peels derived hierarchically porous carbons, J. Taiwan Inst. Chem. Eng. 93 (2018) 543–553, https://doi.org/10.1016/j.jtice.2018.08.038.

[49] W.S. Chen, Y.C. Chen, C.H. Lee, Modified activated carbon for copper ion removal from aqueous solution, Processes 10 (1) (2022), https://doi.org/10.3390/pr10010150.

[50] M.A. Al-Ghouti, Y.S. Al-Degs, New adsorbents based on microemulsion modified diatomite and activated carbon for removing organic and inorganic pollutants from waste lubricants, Chem. Eng. J. 173 (1) (2011) 115–128, https://doi.org/10.1016/j.cej.2011.07.047.

[51] D. Yang, et al., Simultaneous adsorption of Cd(II) and As(III) by a novel biochar-supported nanoscale zero-valent iron in aqueous systems, Sci. Total Environ. 708 (2020) 134823, https://doi.org/10.1016/j.scitotenv.2019.134823.

[52] M.K.M. Nodeh, et al., Strontium oxide decorated iron oxide activated carbon nanocomposite: a new adsorbent for removal of nitrate from well water, J. Braz. Chem. Soc. 31 (1) (2020) 116–125, https://doi.org/10.21577/0103-5053.20190138.

[53] A. Kumar, H.M. Jena, Preparation and characterization of high surface area activated carbon from Fox nut (Euryale ferox) shell by chemical activation with H3PO4, Results Phys. 6 (2016) 651–658, https://doi.org/10.1016/j.rinp.2016.09.012.

[54] K.S. Baig, H.D. Doan, J. Wu, Multicomponent isotherms for biosorption of Ni2+ and Zn2+, Desalination 249 (1) (2009) 429–439, https://doi.org/10.1016/j.desal.2009.06.052.

[55] M. Luo, H. Lin, Y. He, B. Li, Y. Dong, L. Wang, Efficient simultaneous removal of cadmium and arsenic in aqueous solution by titanium-modified ultrasonic biochar, Bioresour. Technol. 284 (February) (2019) 333–339, https://doi.org/10.1016/j.biortech.2019.03.108.

[56] H. Merrikhpour, M. Jalali, Comparative and competitive adsorption of cadmium, copper, nickel, and lead ions by Iranian natural zeolite, Clean Technol. Environ. Policy 15 (2) (2013) 303–316, https://doi.org/10.1007/s10098-012-0522-1.

[57] R. Saikia, et al., Removal of arsenic and fluoride from aqueous solution by biomass based activated biochar: optimization through response surface methodology, J. Environ. Chem. Eng. 5 (6) (2017) 5528–5539, https://doi.org/10.1016/j.jece.2017.10.027.

[58] S.C. Rodrigues, M.C. Silva, J.A. Torres, M.L. Bianchi, Use of magnetic activated carbon in a solid phase extraction procedure for analysis of 2,4-dichlorophenol in water samples, Water. Air. Soil Pollut. 231 (6) (2020), https://doi.org/10.1007/s11270-020-04610-1.

[59] N.K. Kalagatur, et al., Application of activated carbon derived from seed shells of Jatropha curcas for decontamination of zearalenone mycotoxin, Front. Pharmacol. 8 (OCT) (2017) 1–13, https://doi.org/10.3389/fphar.2017.00760.

[60] Buhani, T.A. Wijayanti, Sumadi Suharso, M. Ansori, Application of modified green algae Nannochloropsis sp. as adsorbent in the simultaneous adsorption of Methylene Blue and Cu(II) cations in solution, Sustain. Environ. Res. 31 (1) (2021), https://doi.org/10.1186/s42834-021-00090-y.

[61] V.K. Rathore, D.K. Dohare, P. Mondal, Competitive adsorption between arsenic and fluoride from binary mixture on chemically treated laterite, J. Environ. Chem. Eng. 4 (2) (2016) 2417–2430, https://doi.org/10.1016/j.jece.2016.04.017.

[62] I.H. Çeribasi, U. Yetis, Biosorption of Ni(ii) and Pb(ii) by Phanerochaete chrysosporium from a binary metal system - kinetics, WaterSA 27 (1) (2001) 15–20, https://doi.org/10.4314/wsa.v27i1.5004.

[63] K. Tohdee, L. Kaewsichan, Asadullah, Potential of BCDMACl modified bentonite in simultaneous adsorption of heavy metal Ni (II) and humic acid, J. Environ. Chem. Eng. 6 (4) (2018) 5616–5624, https://doi.org/10.1016/j.jece.2018.08.051.

[64] N. Singh, A. Kumari, C. Balomajumder, Modeling studies on mono and binary component biosorption of phenol and cyanide from aqueous solution onto activated carbon derived from saw dust, Saudi J. Biol. Sci. 25 (7) (2018) 1454–1467, https://doi.org/10.1016/j.sjbs.2016.01.007.

[65] S. Yao, Z. Liu, Z. Shi, Arsenic removal from aqueous solutions by adsorption onto iron oxide/activated carbon magnetic composite, J. Environ. Heal. Sci. Eng. 12 (1) (2014) 6–13, https://doi.org/10.1186/2052-336X-12-58.

[66] D. Banerjee, U. Sarkar, D. Roy, Multicomponent adsorption of chlorhexidine gluconate in presence of a cationic surfactant: role of electrostatic interactions and surface complexation, J. Environ. Chem. Eng. 1 (3) (2013) 241–251, https://doi.org/10.1016/j.jece.2013.05.001.

[67] L.C. Abdullah, Muhammad, S.J. Shima, T.S.Y. Choong, Modelling of single and binary adsorptions of heavy metals onto activated carbon - equilibrium studies, Pertanika J. Sci. Technol. 18 (1) (2010) 83–93.

[68] Z. Zhou, Y. Yu, Z. Ding, M. Zuo, C. Jing, Competitive adsorption of arsenic and fluoride on {2 0 1} TiO 2, Appl. Surf. Sci. 466 (September 2018) (2019) 425–432, https://doi.org/10.1016/j.apsusc.2018.10.052.

[69] V.K. Rathore, P. Mondal, Competitive adsorption of arsenic and fluoride onto economically prepared aluminum oxide/hydroxide nanoparticles: multicomponent isotherms and spent adsorbent management, Ind. Eng. Chem. Res. 56 (28) (2017) 8081–8094, https://doi.org/10.1021/acs.iecr.7b01139.

[70] K. Szewczuk-Karpisz, et al., Simultaneous adsorption of Cu(II) ions and poly(acrylic acid) on the hybrid carbon-mineral nanocomposites with metallic elements, J. Hazard Mater. 412 (January) (2021), https://doi.org/10.1016/j.jhazmat.2021.125138.

[71] J.S. Zhang, R.S. Stanforth, S.O. Pehkonen, Effect of replacing a hydroxyl group with a methyl group on arsenic (V) species adsorption on goethite (α-FeOOH), J. Colloid Interface Sci. 306 (1) (2007) 16–21, https://doi.org/10.1016/j.jcis.2006.10.004.

[72] S.S. Salih, H.N. Mohammed, G.H. Abdullah, M. Kadhom, T.K. Ghosh, Simultaneous removal of Cu(II), Cd(II), and industrial dye onto a composite chitosan biosorbent, J. Polym. Environ. 28 (1) (2020) 354–365, https://doi.org/10.1007/s10924-019-01612-x.

[73] J. Alchouron, et al., Household Arsenic Contaminated Water Treatment Employing Iron Oxide/bamboo Biochar Composite: an Approach to Technology Transfer, vol. 587, Elsevier Inc., 2021, https://doi.org/10.1016/j.jcis.2020.11.036.

[74] K. Wu, et al., Competitive adsorption behaviors of arsenite and fluoride onto manganese-aluminum binary adsorbents, Colloids Surfaces A Physicochem. Eng. Asp. 529 (May) (2017) 185–194, https://doi.org/10.1016/j.colsurfa.2017.05.039.

[75] O.S. Thirunavukkarasu, T. Viraraghavan, K.S. Subramanian, Arsenic removal from drinking water using iron oxide-coated sand, Water. Air. Soil Pollut. 142 (1–4) (2003) 95–111, https://doi.org/10.1023/A:1022073721853.

[76] B. Nath, S. Chakraborty, A. Burnol, D. Stüben, D. Chatterjee, L. Charlet, Mobility of arsenic in the sub-surface environment: an integrated hydrogeochemical study and sorption model of the sandy aquifer materials, J. Hydrol. 364 (3–4) (2009) 236–248, https://doi.org/10.1016/j.jhydrol.2008.10.025.

[77] C.R. Girish, V.R. Murty, Mass transfer studies on adsorption of phenol from wastewater using lantana camara, forest waste, Int. J. Chem. Eng. 2016 (2016), https://doi.org/10.1155/2016/5809505.

[78] A.A. Mohammed, O.A. Abdel Moamen, S.S. Metwally, A.M. El-Kamash, I. Ashour, M.S. Al-Geundi, Utilization of modified attapulgite for the removal of Sr(II), Co(II), and Ni(II) ions from multicomponent system, Part I: kinetic studies, Environ. Sci. Pollut. Res. 27 (7) (2020) 6824–6836, https://doi.org/10.1007/s11356-019-07292-3.

[79] J.B. Arup Roy, A binary and ternary adsorption study of wastewater Cd(II), Ni(II) and Co(II) by c-Fe2O3 nanotubes, Elsevier (2013), https://doi.org/10.1016/j.seppur.2013.05.010.

[80] Z. rong Liu, S. qi Zhou, Adsorption of copper and nickel on Na-bentonite, Process Saf. Environ. Protect. 88 (1) (2010) 62–66, https://doi.org/10.1016/j.psep.2009.09.001.
[81] U. Pongkitdachoti, F. Unob, Simultaneous adsorption of silver nanoparticles and silver ions on large pore mesoporous silica, J. Environ. Chem. Eng. 6 (1) (2018) 596–603, https://doi.org/10.1016/j.jece.2017.12.046.
[82] D.H. Phillips, B. Sen Gupta, S. Mukhopadhyay, A.K. Sen Gupta, Arsenic and fluoride removal from contaminated drinking water with Haix-Fe-Zr and Haix-Zr resin beads, J. Environ. Manage. 215 (2018) 132–142, https://doi.org/10.1016/j.jenvman.2018.03.018.
[83] B. de Paula Ramos, I.D. Perez, M.S. Paiano, M.G.A. Vieira, R.F. Boina, Activated carbons from passion fruit shells in adsorption of multimetal wastewater, Environ. Sci. Pollut. Res. 29 (1) (2022) 1446–1457, https://doi.org/10.1007/s11356-021-15449-2.
[84] A.A. Oladipo, M. Gazi, E. Yilmaz, Single and binary adsorption of azo and anthraquinone dyes by chitosan-based hydrogel: selectivity factor and Box-Behnken process design, Chem. Eng. Res. Des. 104 (2015) 264–279, https://doi.org/10.1016/j.cherd.2015.08.018.
[85] R. DhanaRamalakshmi, M. Murugan, V. Jeyabal, Arsenic removal using Prosopis spicigera L. wood (PsLw) carbon–iron oxide composite, Appl. Water Sci. 10 (9) (2020), https://doi.org/10.1007/s13201-020-01298-w.
[86] Y. Wu, Y. Wen, J. Zhou, J. Cao, Y. Jin, Y. Wu, Comparative and competitive adsorption of Cr(VI), As(III), and Ni(II) onto coconut charcoal, Environ. Sci. Pollut. Res. 20 (4) (2013) 2210–2219, https://doi.org/10.1007/s11356-012-1066-y.
[87] D. Sun, X. Zhang, Y. Wu, T. Liu, Kinetic mechanism of competitive adsorption of disperse dye and anionic dye on fly ash, Int. J. Environ. Sci. Technol. 10 (4) (2013) 799–808, https://doi.org/10.1007/s13762-012-0130-y.
[88] G. Vatankhah, F. Parsa, D. Jafari, M. Esfandyari, Evaluation of adsorptive performance of Mn-doped Fe2O4 nanoparticles loaded on activated carbon in removal of boron ions from synthetic wastewater, Biomass Convers. Biorefinery (2023) 0123456789, https://doi.org/10.1007/s13399-023-04695-8.
[89] E. Aboli, D. Jafari, H. Esmaeili, Heavy metal ions (lead, cobalt, and nickel) biosorption from aqueous solution onto activated carbon prepared from Citrus limetta leaves, Carbon Lett 30 (6) (2020) 683–698, https://doi.org/10.1007/s42823-020-00141-1.
[90] Y. Zhou, et al., Single and simultaneous adsorption of pefloxacin and Cu(II) ions from aqueous solutions by oxidized multiwalled carbon nanotube, Sci. Total Environ. 646 (2019) 29–36, https://doi.org/10.1016/j.scitotenv.2018.07.267.
[91] D. Mohanta, M. Ahmaruzzaman, Bio-inspired adsorption of arsenite and fluoride from aqueous solutions using activated carbon@SnO2 nanocomposites: isotherms, kinetics, thermodynamics, cost estimation and regeneration studies, J. Environ. Chem. Eng. 6 (1) (2018) 356–366, https://doi.org/10.1016/j.jece.2017.11.076.
[92] P. Senthil Kumar, S. Ramalingam, C. Senthamarai, M. Niranjanaa, P. Vijayalakshmi, S. Sivanesan, Adsorption of dye from aqueous solution by cashew nut shell: studies on equilibrium isotherm, kinetics and thermodynamics of interactions, Desalination 261 (1–2) (2010) 52–60, https://doi.org/10.1016/j.desal.2010.05.032.
[93] A.L. Prasad, T. Santhi, S. Manonmani, Recent developments in preparation of activated carbons by microwave: study of residual errors, Arab. J. Chem. 8 (3) (2015) 343–354, https://doi.org/10.1016/j.arabjc.2011.01.020.
[94] T. Khamanur, A. Tg, M. Zamri, M. Sakinah, A. Munaim, Z. Abdul, Regression analysis for the adsorption isotherms of natural dyes onto bamboo yarn, Int. Res. J. Eng. Technol. 4 (6) (2017) 2–6 [Online]. Available: https://irjet.net/archives/V4/i6/IRJET-V4I6321.pdf.
[95] M. Hadi, M.R. Samarghandi, G. McKay, Equilibrium two-parameter isotherms of acid dyes sorption by activated carbons: study of residual errors, Chem. Eng. J. 160 (2) (2010) 408–416, https://doi.org/10.1016/j.cej.2010.03.016.
[96] S. Bibi, A. Farooqi, K. Hussain, N. Haider, Evaluation of industrial based adsorbents for simultaneous removal of arsenic and fluoride from drinking water, J. Clean. Prod. 87 (1) (2015) 882–896, https://doi.org/10.1016/j.jclepro.2014.09.030.
[97] V.K. Rathore, P. Mondal, Stabilization of arsenic and fluoride bearing spent adsorbent in clay bricks: preparation, characterization and leaching studies, J. Environ. Manage. 200 (2017) 160–169, https://doi.org/10.1016/j.jenvman.2017.05.081.
[98] L. Chunhui, T. Jin, Z. Puli, Z. Bin, B. Duo, L. Xuebin, Simultaneous removal of fluoride and arsenic in geothermal water in Tibet using modified yak dung biochar as an adsorbent, R. Soc. Open Sci. 5 (11) (2018), https://doi.org/10.1098/rsos.181266.
[99] P. Dhanasekaran, O. Sahu, Arsenate and fluoride removal from groundwater by sawdust impregnated ferric hydroxide and activated alumina (SFAA), Groundw. Sustain. Dev. 12 (2021) 100490, https://doi.org/10.1016/j.gsd.2020.100490.
[100] J.C. Burillo, L. Ballinas, G. Burillo, E. Guerrero-Lestarjette, D. Lardizabal-Gutierrez, H. Silva-Hidalgo, Chitosan hydrogel synthesis to remove arsenic and fluoride ions from groundwater, J. Hazard Mater. 417 (May) (2021) 126070, https://doi.org/10.1016/j.jhazmat.2021.126070.
[101] T.B. Mlilo, L.R. Brunson, D.A. Sabatini, Arsenic and fluoride removal using simple materials, J. Environ. Eng. 136 (4) (2010) 391–398, https://doi.org/10.1061/(asce)ee.1943-7870.0000154.
[102] Y. Tian, et al., Modified native cellulose fibers-A novel efficient adsorbent for both fluoride and arsenic, J. Hazard Mater. 185 (1) (2011) 93–100, https://doi.org/10.1016/j.jhazmat.2010.09.001.
[103] M. Singanodi, V. Pratheek, C. Nagaraj, A. Kumar, K. Mallikarjunappa, Competitive and cooperative adsorption analysis for dye removal from multicomponent system using Prosopis juliflora activated carbon, Environ. Sci. Pollut. Res. (2022) 0123456789, https://doi.org/10.1007/s11356-022-24721-y.
[104] M.J. Nyangi, Y. Chebude, K.F. Kilulya, A. Minu, Effects of coexisting ions on simultaneous removal of fluoride and arsenic from water by hybrid Al–Fe electrocoagulation, Int. J. Environ. Sci. Technol. 19 (7) (2022) 6667–6680, https://doi.org/10.1007/s13762-021-03598-3.
[105] J.O. Gonçalves, K.A. Silva, G.L. Dotto, L.A.A. Pinto, Adsorption kinetics of dyes in single and binary systems using cyanoguanidine-crosslinked chitosan of different deacetylation degrees, J. Polym. Environ. 26 (6) (2018) 2401–2409, https://doi.org/10.1007/s10924-017-1133-z.
[106] S. Sohn, D. Kim, Modification of Langmuir Isotherm in Solution Systems — Definition and Utilization of Concentration Dependent Factor, vol. 58, 2005, pp. 115–123, https://doi.org/10.1016/j.chemosphere.2004.08.091.
[107] T.C. Prathna, S.K. Sharma, M. Kennedy, Arsenic and fluoride removal by iron oxide and iron oxide/alumina nanocomposites: a comparison, Proc. World Congr. New Technol. (2017) 1–4, https://doi.org/10.11159/icnfa17.118.
[108] S. Chouhan, S.J.S. Flora, Arsenic and fluoride: two major ground water pollutants, Indian J. Exp. Biol. 48 (7) (2010) 666–678.
[109] H. Saitua, R. Gil, A.P. Padilla, Experimental investigation on arsenic removal with a nanofiltration pilot plant from naturally contaminated groundwater, Desalination 274 (1–3) (2011) 1–6, https://doi.org/10.1016/j.desal.2011.02.044.
[110] A.P. Padilla, H. Saitua, Performance of simultaneous arsenic, fluoride and alkalinity (bicarbonate) rejection by pilot-scale nanofiltration, Desalination 257 (1–3) (2010) 16–21, https://doi.org/10.1016/j.desal.2010.03.022.
[111] T. Şahan, Application of RSM for Pb(II) and Cu(II) adsorption by bentonite enriched with [sbnd]SH groups and a binary system study, J. Water Process Eng. 31 (May) (2019), https://doi.org/10.1016/j.jwpe.2019.100867.